Starburst radio galaxies: general properties, evolutionary histories and triggering

C. Tadhunter,[1]* J. Holt,[2] R. González Delgado,[3] J. Rodríguez Zaurín,[4]
M. Villar-Martín,[3] R. Morganti,[5] B. Emonts,[6] C. Ramos Almeida[1] and K. Inskip[7]

[1]*Department of Physics and Astronomy, University of Sheffield, Sheffield S3 7RH*
[2]*Leiden Observatory, Leiden University, PO Box 9513, 2300 RA Leiden, the Netherlands*
[3]*Instituto de Astrofísica de Andalucía (CSIC), Apdo. 3004, 18080 Granada, Spain*
[4]*DAMIR, Instituto de Estructura de la Materia, CSIC, Madrid, Spain*
[5]*ASTRON, PO Box 2, 7990 AA Dwingeloo, the Netherlands*
[6]*CSIRO Astronomy and Space Science, Australia Telescope National Facility, PO Box 76, Epping, NSW 1710, Australia*
[7]*Max-Planck-Institut für Astronomie, Königstuhl 17, D-69117 Heidelberg, Germany*

ABSTRACT

In this paper we discuss the results of a programme of spectral synthesis modelling of a sample of starburst radio galaxies in the context of scenarios for the triggering of the activity and the evolution of the host galaxies. New optical spectra are also presented for a subset of the objects discussed. The starburst radio galaxies – comprising $\sim$15–25 per cent of all powerful extragalactic radio sources – frequently show disturbed morphologies at optical wavelengths, and unusual radio structures, although their stellar masses are typical of radio galaxies as a class. In terms of the characteristic ages of their young stellar populations (YSPs), the objects can be divided into two groups: those with YSP ages $t_{YSP} \leq 0.1$ Gyr, in which the radio source has been triggered quasi-simultaneously with the main starburst episode, and those with older YSP in which the radio source has been triggered or re-triggered a significant period after the starburst episode. Most of the former group are associated with a large mid- to far-IR (MFIR) continuum and [O III] emission-line luminosities ($L_{IR} > 10^{11}$ L$_\odot$, $L_{[O III]} > 10^{35}$ W), while most of the latter have lower luminosities. Combining the information on the YSP with that on the optical morphologies of the host galaxies, we deduce that the majority of the starburst radio galaxies have been triggered in galaxy mergers in which at least one of the galaxies is gas rich. However, the triggering (or re-triggering) of the radio jets can occur immediately before, around or a significant period after the final coalescence of the merging nuclei, reflecting the complex gas infall histories of the merger events. Although $\sim$25 per cent of starburst radio galaxies are sufficiently bright at MFIR wavelengths to be classified as ultraluminous infrared galaxies (ULIRGs), we show that only the most massive ULIRGs are capable of evolving into radio galaxies. Finally, for a small subset of starburst radio galaxies in rich clusters of galaxies, cooling flows associated with the hot X-ray haloes offer a viable alternative to mergers as a trigger for the radio jet activity. Overall, our results provide further evidence that a powerful radio jet activity can be triggered via a variety of mechanisms, including different evolutionary stages of major galaxy mergers; clearly, radio-loud AGN activity is not solely associated with a particular stage of a unique type of gas accretion event.

Key words: galaxies: active – galaxies: interactions – galaxies: jets – galaxies: starburst.

1 INTRODUCTION

Active galactic nuclei (AGN) are increasingly recognized as a key element in the overall galaxy evolution process (e.g. Cattaneo et al. 2009), yet the nature of the link between AGN and galaxy evolution

*E-mail: c.tadhunter@sheffield.ac.uk

is not understood in-depth. The link can take two main forms: the triggering of AGN as gas is driven into the nuclear regions of galaxies as they evolve; and the direct impact of the AGN-driven outflows on the ISM in the galaxy bulges, haloes and any surrounding groups and clusters. The latter AGN feedback effect has been invoked to explain the correlations between black hole mass and host galaxy properties (e.g. Silk & Rees 1998; Fabian 1999; di Matteo, Springel & Hernquist 2005; Bower et al. 2006), as well as the high-end shape of the galaxy luminosity function (Benson et al. 2003). On the other hand, the triggering of AGN activity as a result of evolution-driven gas accretion can provide an explanation for the similarity between the redshift evolution of AGN activity and that of the global star formation rate of the field galaxy population (Dunlop & Peacock 1990; Madau et al. 1996). Clearly, if we are to incorporate the AGN feedback effect accurately into galaxy evolution models, it is important to understand how and when AGN are triggered as their host galaxies evolve.

Deep ground-based imaging observations of powerful radio galaxies show morphological evidence (tidal tails, fans, bridges and shells etc.) that a large fraction are triggered in galaxy interactions and mergers (Heckman et al. 1986; Smith & Heckman 1989; Ramos Almeida et al. 2010a). A merger origin is also supported by the kinematics of the extended emission-line regions in some sources (Tadhunter, Fosbury & Quinn 1989; Baum, Heckman & van Breugel 1992). However, the idea that the activity is always triggered in major galaxy mergers and interactions has been challenged by high-resolution *Hubble Space Telescope* (*HST*) images which provide evidence that the host galaxies of powerful AGN of both radio-loud and radio-quiet types are relatively quiescent giant elliptical galaxies (Dunlop et al. 2003). At least part of this apparent discrepancy between the *HST* and ground-based results is likely to be a consequence of the fact that shallow *HST* observations are sensitive to high surface brightness structures close to the nuclei, while the lower-resolution ground-based studies are more sensitive to lower surface brightness structures on larger scales (see discussion in Canalizo et al. 2007; Bennert et al. 2008).

While some radio galaxies show clear evidence for triggering in galaxy interactions and mergers, a significant subset have optical morphologies and emission line kinematics that do not support such a triggering mechanism. Many such cases are central cluster galaxies surrounded by massive haloes of hot gas (Tadhunter et al. 1989; Baum et al. 1992). Therefore, the infall of warm/cool gas condensing from the hot X-ray haloes in cooling flows has been been suggested as an alternative trigger for the AGN activity (e.g. Bremer, Fabian & Crawford 1997). In addition, based both on detailed X-ray studies of individual objects and optical studies of large samples of low-luminosity radio sources, the direct (Bondi) accretion of the *hot* ISM associated with the X-ray haloes has been proposed to explain the fuelling of weak line radio galaxies (WLRG) in the local Universe (Best et al. 2005; Allen et al. 2006; Best et al. 2006; Hardcastle, Evans & Croston 2007; Buttiglione et al. 2010).

Although the morphologies and emission line kinematics provide important information about the triggering events, this information is generally qualitative. For example, it is difficult to use such information to quantify when AGN are triggered in major galaxy mergers relative to the time of coalescence of the merging nuclei. Fortunately, another facet of the gas accretion events that trigger AGN activity is that they are also likely to be associated with star formation in the host galaxies; therefore, by studying the young stellar populations in the predominantly early-type host galaxies of powerful radio sources, we can obtain key information about the nature of the triggering events.

Substantial recent progress has been made in quantifying the degree of recent star formation activity in radio galaxies using both optical/UV observations of direct starlight (Tadhunter et al. 2002; Wills et al. 2002, 2004; Raimann et al. 2005; Baldi & Capetti 2008) and far-IR observations of dust-reprocessed starlight (Tadhunter et al. 2007; Dicken et al. 2008, 2009). Concentrating on optical/UV spectroscopic studies of complete samples that take full account of contamination of the continuum by AGN-related components (e.g. scattered or direct AGN light, nebular continuum), as well as intrinsic reddening of the starlight, young stellar populations (YSPs) are detected spectroscopically in 15–30 per cent of powerful 2 Jy and 3CR radio galaxies at low and intermediate redshifts (Tadhunter et al. 2002; Wills et al. 2002, 2004; Holt et al. 2007); the major uncertainties in these numbers are due to objects in which the strength of the direct or scattered AGN component makes detection of the YSP difficult. Despite the possibility that a substantial proportion of YSP emission may be absorbed by dust at optical/UV wavelengths, analysis of the mid- to far-IR (MFIR) continuum properties of powerful radio galaxies derived from deep *Spitzer* observations yields a similar proportion of powerful radio galaxies with energetically significant recent star formation activity (∼15–28 per cent: Tadhunter et al. 2007; Dicken et al. 2008; 2009).[1]

The identification of YSP in a significant fraction of nearby radio galaxies has opened the possibility of using spectral synthesis modelling of the stellar populations to investigate the AGN-triggering events and the evolution of the host galaxies. Initial results provided a mixed picture. On one hand, Tadhunter et al. (2005) and Emonts et al. (2006) found evidence for intermediate YSP ages in their small sample of four nearby radio galaxies, pointing to a significant delay between the starbursts and the AGN activity, similar to those reported for samples of star-forming galaxies and radio-quiet AGN in the local Universe (e.g. Davies et al. 2007; Wild, Heckman & Charlot 2010). On the other hand, a detailed study by Wills et al. (2008) of two intermediate redshift radio galaxies demonstrated the presence of much younger stellar populations in one object, as well as intermediate-age stellar populations in both objects. All the spectral synthesis modelling studies of radio galaxies have stressed the following common features.

(i) *Masses.* The masses associated with the YSP detected spectroscopically in radio galaxies are significant ($1 \times 10^9 < M_{\mathrm{YSP}} < 5 \times 10^{10}$ M$_\odot$), amounting to typically 1–40 per cent of the total stellar masses of the host galaxies; if the starbursts and AGN are triggered in mergers, then the systems with the more massive YSP must be associated with relatively major mergers, in which at least one of the merging galaxies is gas rich.

(ii) *Spatial distribution.* When substantial YSP are detected in the nuclear regions of the radio galaxies, in general they are also detected across the full extents of the galaxies over which it is possible to make spectroscopic observations with the high signal-to-noise ratio (S/N) required for spectral synthesis modelling (e.g. Holt et al. 2007). In some cases, the YSP are detected on scales of 10s of kpc. Again this is consistent with simulations of gas-rich

---

[1] *HST* imaging observations at UV wavelengths show evidence for YSP in a higher proportion of radio galaxies with strong emission lines (Baldi & Capetti 2008). However, since the level of dilution by the light of the old stellar populations of the host galaxies is more than a factor of ×10 less at UV wavelengths than optical wavelengths, such observations are sensitive to relatively low levels of recent star formation activity that may be insignificant in terms of their contribution to the masses and energetics of the host galaxies.

mergers that predict galaxy-wide star formation activity (e.g. Mihos & Hernquist 1996; Barnes 2004), although it does not preclude other triggering mechanisms.

(iii) *Reddening.* Reddening of the optical/UV light of the YSP by dust is important, especially in the nuclear regions of the galaxies [typically $0.4 < E(B - V) < 1.0$]; failure to take such reddening into account leads to inaccurate ages for the YSP and, in particular, to the overestimation of the ages of the YSP.

In this paper we draw together and summarize the results of all the recent spectral synthesis studies of radio galaxies that are based on high-quality optical spectra, including the recent investigation of 12 low- and intermediate-redshift radio galaxies by Holt et al. (2007). New spectral synthesis results are also presented for a subset of the sample. The properties of the YSP are then discussed in the context of the morphologies of the host galaxies, in order to investigate the nature, the time-scales and the order of events of the triggering of the activity of an important subset of the population of galaxies with powerful AGN. Throughout this paper we assume a cosmology with $H_0 = 72 \, \mathrm{km \, s^{-1}}$, $\Omega_{\mathrm{m}} = 0.27$ and $\Omega_{\Lambda} = 0.73$.

2 SAMPLE SELECTION AND SPECTRAL SYNTHESIS MODELLING

Optical and MFIR observations provide evidence for recent star formation activity in up to 30 per cent of all radio galaxies. However, in this paper we concentrate on the $\sim$15–25 per cent of the radio galaxy population with clear, unambiguous evidence for young stellar populations at optical wavelengths, which have been modelled using spectral synthesis techniques that take full account of the reddening and potential AGN contamination. These latter criteria are important because of the known contamination by scattered or direct AGN light and/or nebular continuum from the NLR in some objects, the strong evidence that the YSP in the nuclear regions are significantly reddened in many cases, and potential degeneracy issues when more than one stellar population is present (see Tadhunter et al. 2002; Holt et al. 2007; Wills et al. 2008, for a full discussion of these issues). Our sample comprises all 18 of the objects fulfilling these selection criteria from our own detailed studies of nearby 2Jy, 3CR and B2 radio galaxies (Tadhunter et al. 2005; Emonts et al. 2006; Holt et al. 2007; Wills et al. 2008),[2] along with 3C48, which has been modelled using a similar approach.[3] In addition, we include a further two nearby objects from the literature with good spectroscopic observations of individual star clusters (Centaurus A and Fornax A); such clusters do not suffer from the degeneracy issues associated with multiple stellar populations and AGN contamination. For convenience we label all the objects in our sample collectively as 'starburst radio galaxies', with the caveat that in some cases the star formation histories may have been more complex than a single starburst.

Although not in any sense complete, our sample includes all seven (15 per cent) of the 2Jy sample of 46 southern radio galaxies

with intermediate redshifts ($0.05 < z < 0.7$) described in Dicken et al. (2008), and all five (25 per cent) of the low-redshift ($z < 0.1$) sample of 19 3CRR FRII radio galaxies described in Dicken et al. (2010), that show strong evidence for recent star formation activity at optical wavelengths. Therefore, it is representative of the most extreme star-forming radio galaxies in the local Universe; in these objects the YSP typically contribute >20 per cent of the total light at $\sim$4800 Å. We emphasize that lower levels of star formation activity may be present in a larger fraction of the local radio galaxy population, but not clearly detected at optical wavelengths because of dilution by the light of the old stellar populations of the host galaxies and/or AGN-related continuum components.

The general properties of the starburst radio galaxies are presented in Table 1, while the properties of their YSP, as derived from spectral synthesis modelling, are detailed in Table 2. Note that, with the exception of the individual star clusters in Cen A and Fornax A, the results presented in Table 2 refer to the simplest models that provide an adequate fit to the overall optical/near-UV SEDs and detailed absorption features (see Holt et al. 2007; Wills et al. 2008, for a detailed description of the modelling approach). These comprise a reddened YSP combined with an unreddened old stellar population (OSP: $t_{\mathrm{OSP}} > 5 \, \mathrm{Gyr}$). Because of the potential degeneracy issues, related to the relatively large contribution from OSP and reddening of the YSP, more detailed fits are not, in general, warranted. The exception is the case of 3C 459 discussed by Wills et al. (2008) in which the dominance of the young stellar component relative to the OSP allows two YSP components of different age (young: $t_{\mathrm{YSP}} < 0.1 \, \mathrm{Gyr}$; and intermediate: $0.3 < t_{\mathrm{YSP}} < 0.9 \, \mathrm{Gyr}$) to be fitted to the data, although the results in Table 2 for that object refer to the single reddened YSP plus OSP fit. Overall, the results presented in Table 2 represent the luminosity-weighted ages of the YSP present in each system.

3 NEW SPECTROSCOPIC OBSERVATIONS

In addition to spectroscopic observations already reported in the literature and described in the Appendix of this paper, new spectra for some of the starburst radio galaxies were obtained in various runs on the ESO Very Large Telescope (VLT), 3.6-m and New Technology Telescope (NTT) telescopes. Details of these new observations are given in Table 3. The reduction of these data followed the standard steps of bias subtraction, flat fielding, wavelength calibration, atmospheric extinction correction, flux calibration and registration of blue and red spectral images. Based on measurements of night sky lines, the uncertainty in the wavelength calibration is estimated to be smaller than 0.5 Å for all data sets; the relative flux calibration uncertainty, based on the comparison of observations of several spectroscopic standard stars, is better than ±5 per cent. Prior to the analysis of the data, the spectra were corrected for Galactic extinction using values of $E(B - V)$ derived from Schlegel, Finkbeiner & Davis (1998) along with the Seaton (1979) extinction law. Note that, in the cases of the VLT/FORS1 observations of PKS0023-26 and PKS1549-79, the data were taken in spectropolarimetric mode with the light passing through a half-wave plate as well as an analysing prism. In the latter two cases, the 'o' and 'e' ray images of the long-slit spectra were spatially registered and co-added, and the flux calibration was performed using spectropolarimetric standard stars observed through the same instrument configuration as the target galaxies.

For some of the objects discussed in this paper (Fornax A, PKS0652-20, PKS1549-79) we have carried out new spectral synthesis modelling in an attempt to improve our knowledge of the

---

[2] In all of these studies we used the instantaneous burst, solar metallicity spectral synthesis results of Bruzual & Charlot (2003) to model the spectra.
[3] Note that, although Canalizo & Stockton (2000) and Stockton et al. (2007) did not consider the effects of reddening in their study of the YSP in this luminous quasar, the regions studied are well separated from the nucleus and dominated by the light of young/intermediate-age YSPs. Therefore, degeneracy issues are likely to be less severe than in some near-nuclear regions where old stellar populations make a larger contribution, and the ages derived using unreddened templates are likely to be accurate.

Table 1. The general properties of the objects discussed in this paper. The integrated mid- to far-IR (MFIR) luminosities presented in column 3 have been estimated from published IRAS and *Spitzer* flux data using the formulae given in Sanders & Mirabel (1996). Key for the optical morphology: E, elliptical; S0, S0 galaxy; A, amorphous halo; CE common, envelope with companion galaxies; D, dust lane; 2N, double nucleus; TT, tidal tail(s); S, shell(s); DE, distorted envelope; B, bridge to companion galaxy; F, fan(s); R, ring structure. Key for radio morphology: FRI, Fanaroff Riley class I; FRII, Fanaroff Riley class II; CSS, compact steep spectrum radio source; GPS, giga-hertz peak radio source; CFS, compact flat spectrum radio source; DD, double–double radio structure; HSBI+DO, high surface brightness inner structure plus diffuse outer structure; SSC, steep spectrum core structure. Note that the radio morphological classifications were made by CT, based on published radio maps.

Object	Redshift	$P_{5\,GHz}$ (W Hz^{-1})	$L_{[O\,III]}$ (W)	L_{IR} (L$_\odot$)	Optical morphology	Radio morphology
PKS0023−26	0.322	1.1×10^{27}	1.5×10^{35}	1.5×10^{11}	E, A, CE	CSS
NGC 612	0.030	7.9×10^{24}	5.6×10^{32}	1.1×10^{11}	S0, D, S	FRI/FRII
3C 48	0.367	3.6×10^{26}	6.8×10^{36}	1.0×10^{13}	Q, 2N, A, TT	CSS
Fornax A	0.006	5.6×10^{24}	$<6.8 \times 10^{31}$	6.0×10^{9}	E/S0, D, S	FRII
PKS0409−75	0.693	8.7×10^{27}	1.3×10^{35}	5.3×10^{11}	E, 2N	FRII
B2 0648+27	0.041	1.9×10^{23}	2.7×10^{34}	2.6×10^{11}	E, R, DE, TT	CSS
PKS0620−52	0.0511	7.4×10^{24}	$<2.5 \times 19^{32}$	2.6×10^{10}	E	FRI
3C 213.1	0.194	7.0×10^{25}	1.3×10^{34}	$<1.9 \times 10^{11}$	E, DE	FRI/FRII, DD
3C 218	0.055	9.5×10^{25}	2.9×10^{33}	2.1×10^{10}	E, D	FRI, HSBI+DO
3C 236	0.101	4.1×10^{25}	3.8×10^{33}	4.1×10^{10}	E, S, D, TT, DE	FRII, DD
3C 285	0.079	9.2×10^{24}	7.0×10^{33}	1.1×10^{11}	E, TT, F, B	FRII
Centaurus A	3.4 Mpc	5.4×10^{23}	1.1×10^{34}	1.0×10^{10}	E/S0, D, S, R	FRI, HSBI+DO
PKS1345+12	0.122	1.0×10^{26}	2.0×10^{35}	1.9×10^{12}	E, 2N, D, TT	GPS, HSBI+DO
3C 293	0.045	9.0×10^{24}	2.9×10^{32}	3.7×10^{10}	E/S0, TT, D, B	FRI/FRII, HSBI+DO
3C 305	0.041	4.3×10^{24}	7.0×10^{33}	3.2×10^{10}	E/S0, TT, D	CSS
3C 321	0.096	2.7×10^{25}	1.3×10^{35}	6.0×10^{11}	E, 2N, TT, S, F	FRII, SSC
PKS1549−79	0.152	2.5×10^{26}	1.0×10^{35}	2.2×10^{12}	E, TT, D	CSS/CFS
PKS1932−46	0.231	5.4×10^{26}	2.5×10^{35}	6.3×10^{10}	E, S, A	FRII
3C 433	0.106	9.5×10^{25}	5.0×10^{34}	3.3×10^{11}	E, A, CE, D	FRI/FRII, SSC
PKS2135−209	0.636	2.5×10^{27}	1.4×10^{36}	1.3×10^{12}	Q, F	CSS
3C 459	0.220	1.8×10^{26}	1.6×10^{35}	1.7×10^{12}	E, F, DE	FRII, SSC

properties of the YSPs. In these cases we followed the procedures outlined in Tadhunter et al. (2005), Holt et al. (2007) and Wills et al. (2008): modelling the continuum spectrum using a combination of a reddened YSP [$0.005 < t_{YSP} < 5$ Gyr, $0 < E(B − V) < 2.0$] and an unreddened OSP ($t_{YSP} = 12.5$ Gyr), taking full account of AGN continuum components (where appropriate). In all cases we used instantaneous burst, solar metallicity spectral synthesis templates from Bruzual & Charlot (2003).

4 GENERAL PATTERNS AND RESULTS

Detailed discussions of the individual starburst radio galaxies, including the new spectroscopic results, are presented in the Appendix. In this section we consider the general results and patterns obtained for the population of starburst radio galaxies as a whole.

4.1 Radio morphologies

It is striking that a large proportion of starburst radio galaxies show unusual radio morphologies that place them outside the regular FRI/FRII morphological classification for extended radio sources: seven (33 per cent) are compact steep spectrum (CSS) or gigahertz peaked (GPS) sources whose radio structures are dominated by structures with a diameter $D < 15$ kpc (PKS0023-26, 3C 48, B2 0648+27, PKS1345+12, 3C 305, PKS1549-79, PKS2135-209); three (14 per cent) show unusually prominent compact steep spectrum core components on a scale of $D < 10$ kpc, even if their radio emission is dominated by radio lobes and hotspots on a larger scale (3C 321, 3C 433, 3C 459); six (29 per cent) show inner high surface brightness steep spectrum structures along with lower surface

brightness outer haloes or double structures (3C 213.1, 3C 218, 3C 236, Cen A, PKS1345+12, 3C 293); and 15 (71 per cent) show one or more of these peculiarities. For comparison, the rate of detection of such features in the southern 2Jy sample of radio galaxies with redshifts in the range $0.05 < z < 0.7$ (see Dicken et al. 2008 for sample definition) is only 28 per cent.

Although our small sample size makes it difficult to find clear trends in the detailed radio morphologies with the properties of the stellar populations, it is notable that all but one (3C 305) of the seven CSS/GPS sources in our sample have nuclear spectra that are consistent with relatively young ages for their YSP ($t_{YSP} < 0.1$ Gyr).

4.2 Optical morphologies

At optical wavelengths most of the objects in our sample of starburst radio galaxies show morphological peculiarities compared with quiescent elliptical galaxies: 17 (80 per cent) show tidal tails, fans or highly asymmetric/clumpy outer envelopes at relatively high surface brightness levels; 14 (67 per cent) show dust features; five (23 per cent) have double nuclei or close companions within 15 kpc; and 20 (95 per cent) show one or more of these optical peculiarities. This rate of incidence is much higher than in the general population of massive elliptical galaxies observed with a similar surface brightness sensitivity (e.g. Malin & Carter 1983). However, at this relatively crude level of morphological classification, a similar rate of morphological disturbance has recently been found in the general population of powerful 2 Jy radio galaxies at intermediate redshifts (including non-starburst objects: Ramos Almeida et al. 2010a).

Table 2. The properties of the young stellar populations in the radio galaxies listed in Table 1. The second column indicates the aperture (N: nuclear; E: extended). The references in column 6 are for the modelling of the young stellar populations: 1. Holt et al. (2007); 2. Stockton et al. (2007); 3. Canalizo & Stockton (2000); 4. Goudfrooij et al. (2001); 5. Kuntschner (2000); 6. this paper; 7. Emonts et al. (2006); 8. O'Dea et al. (2001); 9. Holt et al. (2006); 10. Wills et al. (2008); 11. Villar-Martin et al. (2005); 12. Peng et al. (2002); 13. Peng, Ford & Freeman (2004); 14. Tadhunter et al. (2005); 15. Rodríguez-Zaurín, Tadhunter & González-Delgado (2009).

Object	Region	YSP age (Gyr)	YSP reddening $E(B-V)$	Comment	References
PKS0023−26	N	0.03–0.05	0.9–0.7		1
NGC 612	N	0.05–0.1	1.4–1.2		1
	E: A–F	0.04–0.2	1.0–0.0	Extended disc	1
3C 48	E: 3C 48 A	0.14	0	Secondary nucleus	2
	E: A, B, C, G	0.005–0.114	–	Several regions, four slits	3
Fornax A	E	2.5–3.5	–	Luminous star clusters	4
	E	2.0	–	Diffuse light, line index work, luminosity weighted	5
	N, E	0–2	0–1.5	Diffuse light, SED modelling	6
PKS0409−75	N	0.01–0.04	0.9–0.5	–	1
B2 0648+27	N	0.2–0.4	0.2–0.4	–	7
	E: NE	0.3–0.6	0.0–0.1		7
	E: SW	0.3–0.6	0.0–0.1		7
PKS0620−52	N	0.001–0.9	0.0–1.5	–	6
3C 213.1	N	0.4–0.8	0.1–0.0	–	10
3C 218	N	0.05	0.4	–	1
3C 236	N	0.04–1.0	1.6–0.6	–	1
	E	0.01, 0.1–1	–	Extended star formation complexes, photometric	8
3C 285	N	0.1–0.5	0.2–0.0	–	1
Centaurus A	E	0.35	–	Blue tidal stream	12
	E	2–8	–	Globular cluster system	13
PKS1345+12	N	≤0.06	0.8–1.3	–	15
	E, E1	0.5–1.5	–	–	14
3C 293	N	1.0–2.5	0.5–0.2	–	14
	E, E1	0.1–0.5	–	–	14
	E, E2	1.0–2.5	–	–	14
3C 305	N	0.4–1.0	0.8–0.4	–	14
	E1	0.5–1.5	–	–	14
	E2	0.5–1.0	–	–	14
3C 321	N, SE	0.1–1.0	0.3–0.1	–	1
	N, NW	0.1–1.4	0.3–0.1	Radio source host	1
	E	0.4–1.0	0.1–0.0	Extended regions between nuclei and to SE	1
PKS1549−79	N	0.04–0.1	0.75–0.0	–	9
	E	0.04–0.08	0.4–0.0	Extended envelope to S	6
PKS1932−46	E	<0.01	–	Extended star-forming halo detected in emission lines	11
3C 433	N, SW	0.03–0.1	0.7–0.4	Radio source host	1
	N, NE	0.03–1.4	0.9–0.3	Companion galaxy	1
	E, mid	0.05–1.0	0.7–0.0	Mid way between 3C 433 & companion	1
PKS2135−209	N	0.04–0.6	0.5–0.2	Quasar nucleus modelled with power-law	1
PKS2314+03	N	0.04–0.07	0.4–0.0	–	10
	E, N	0.5–0.7	0.3–0.0	Fit includes a power-law	10
	E, E	0.5–0.6	0.2–0.0	Fit includes a power-law	10

4.3 YSP ages

The ages of the YSPs detected in radio galaxies can provide key information about the order of events and the triggering of the AGN/jet activity. Therefore, it is interesting to examine the distribution of luminosity-weighted YSP ages determined from the two component fits to the optical spectra of the full sample of starburst radio galaxies described in Section 2. The top panel of Fig. 1 shows the distribution of luminosity-weighted ages for the nuclear apertures[4] of the starburst radio galaxies. For comparison we also show the YSP age distribution for a complete sample of ULIRGs with redshifts $z < 0.13$ – representing the extreme starburst population in the local Universe – which have been modelled using identical techniques by Rodríguez Zaurín et al. (2009). Note that, in some apertures of some starburst radio galaxies it proved possible to model the optical spectra with YSP covering a wide range of ages. In such cases we have used the mean age over the range of models that provided good fits. Since the upper limiting ages in the latter group were often large (>1 Gyr), this will tend to skew the age distribution to larger ages.

Several features are apparent from Table 2 and Fig. 1.

---

[4] The exceptions are: 3C 48, for which we have included the information about the YSP ages from the extended apertures modelled by Canalizo & Stockton (2000); Centaurus A for which we have taken the YSP age information for the blue tidal stream extending up to 8 kpc from the nucleus; and Fornax A for which we have used the age estimates for the blue globular clusters in the halo of the galaxy.

Table 3. New spectroscopic observations.

Object	Date	Tel/Inst	Grism	Exposure time (s)	Slit width (arcsec)	Seeing FWHM (arcsec)
PKS0023-26	24/07/03	VLT/FORS1	GRIS-600R	5580	1.3	0.70
Fornax A	7/12/02	NTT/EMMI	Gr5	900	1.0	1.1
	"	"	Gr6	900	"	"
PKS0620-52	16/02/07	ESO3.6m/EFOSC	Gr7	3600	1.2	1.7
	"	"	Gr4	1800	"	"
PKS1549-79	24/07/03	VLT/FORS1	GRIS-600B	5880	1.3	0.65

(i) *Nuclear apertures.* Considering the nuclear apertures (Fig. 1, top), nine (43 per cent) of sources have relatively young YSP ages: $t_{YSP} < 0.1$ Gyr. This group is interesting because the typical time-scale of the starburst in a major galaxy merger is ∼0.1 Gyr (e.g. Rodríguez-Zaurín, Tadhunter & González-Delgado 2010), and powerful extragalactic radio sources are generally considered to have maximum lifetimes in the range of 0.01–0.1 Gyr. For such objects the results are consistent with the starburst and AGN/jet activity occurring quasi-simultaneously, with little evidence for a major time lag between the starburst and the AGN/jet activity. On the other hand, there is also a group of eight objects (36 per cent of sample) with well-determined older YSP ages ($0.3 < t_{YSP} < 3$ Gyr), in which the AGN/jet activity appears to have been triggered or re-triggered a significant period *after* the major star formation episode in the nuclear regions (see also the discussion in Section 5.1). The latter group includes 3C 305 and 3C 293, which were discussed in detail in Tadhunter et al. (2005).

(ii) *Extended versus nuclear apertures.* Considering only the apertures with well-determined YSP ages, there is little evidence for a gradient in the YSP ages from the nuclear to the extended regions; in most cases the nuclear and extended apertures have luminosity-weighted YSP ages that are consistent given the (sometimes large) uncertainties. The exception is 3C 459 for which the intermediate-aged YSP component becomes more significant off-nucleus (Wills et al. 2008), in common with the trend found for other ULIRGs in the local Universe (Rodríguez Zaurín et al. 2009).

(iii) *Comparison with ULIRG YSP ages.* The overwhelming majority of nuclear apertures in the ULIRGs modelled by Rodríguez Zaurín et al. (2009) yield relatively young luminosity-weighted YSP ages: 88 per cent have YSP ages $t_{YSP} < 0.1$ (Fig. 1, bottom). This is consistent with the group of nine radio galaxies identified above with younger YSP ages. Indeed, four of the radio galaxies with younger YSP ages – 3C 48, PKS1345+12, PKS1549-79, 3C 459 – qualify as ULIRGs based on their far-infrared luminosities.
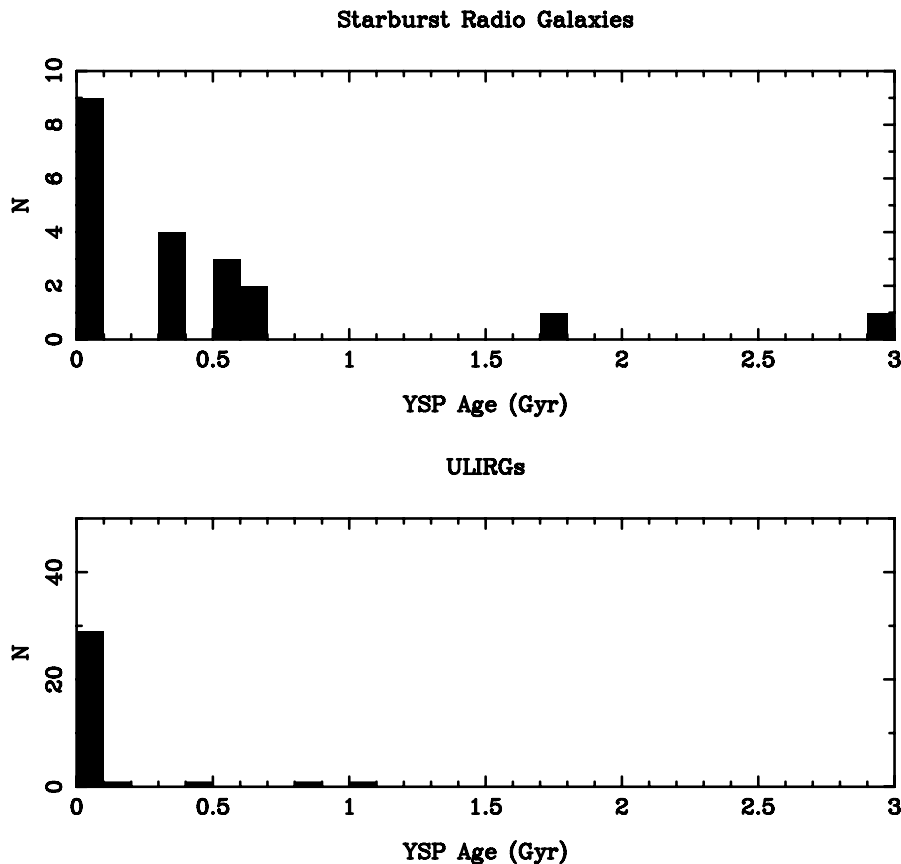
Figure 1. The ages of the YSP in starburst radio galaxies (top), compared with those of $z < 0.13$ ULIRGs from Rodríguez Zaurín et al. (2009) (bottom).

Table 4. Estimated stellar masses for starburst radio galaxies. The second column gives the age and reddening of the YSP in the model used to derive the masses; the third column gives the type of magnitude used to scale the models, with reference to the magnitude in the fourth column; the fifth, sixth and seventh columns give the YSP, OSP and total stellar masses (12.5 Gyr OSP age assumed for all cases, except the higher-redshift objects PKS0409−75 and PKS2135−20, for which a 7.0 Gyr OSP was assumed); and the final column gives the proportional contribution of the YSP to the total stellar mass. Note that in the cases of Fornax A, Centaurus A and PKS1932−46 we do not have an estimate of the proportional contribution of the YSP to the total stellar light. In these cases we have assumed that the starlight is dominated by old stellar populations. * For 3C 48 we have assumed that model B8 from Canalizo & Stockton (2000) is representative of the stellar populations in the host galaxy as a whole. Key for photometry references: 1. Ramos Almeida et al. (2010); 2. RC2; 3. Boyce, Disney & Bleaken (1999); 4. Persson, Frogel & Aaronson (1979); 5. González-Serrano & Caballo (2000); 6. Sloan Digital Sky Survey DR6 (magnitude derived from CMODEL fit); 7. Govoni, Feretti & Giovannini (2000); 8. Lauberts & Valentijn (1989); 9. Drake, McGregor & Dopita (2004); 10. Smith & Heckman (1989); 11. Kim, Veilleux & Sanders (2002).

Object	YSP model (Age, $E(B-V)$)	Mag type	Ref	M_{YSP} ($M_\odot$)	M_{OSP} ($M_\odot$)	M_{tot} ($M_\odot$)	YSP mass contr.
PKS0023−26	(0.03,0.9)	r'	1	6.0×10^{10}	2.9×10^{11}	3.5×10^{11}	17 per cent
NGC 612	(0.05,1.2)	V_T	2	1.6×10^{11}	7.5×10^{11}	9.1×10^{11}	18 per cent
3C 48	(0.1,0)*	F555W	3	1.5×10^{10}	6.6×10^{11}	6.8×10^{11}	2 per cent
Fornax A	–	R_J	4	–	8.3×10^{11}	8.3×10^{11}	–
PKS0409−75	(0.02,0.7)	i'	1	3.8×10^{10}	7.1×10^{11}	7.5×10^{11}	5 per cent
PKS0620−52	(0.7,0.0)	R_c	7	2.3×10^{10}	1.6×10^{12}	1.6×10^{12}	1 per cent
B20648+27	(0.3,0.3)	m_v	5	1.1×10^{11}	2.8×10^{11}	3.9×10^{11}	28 per cent
3C 213.1	(0.6,0.0)	r'	6	2.1×10^{10}	1.7×10^{11}	1.9×10^{11}	11 per cent
3C 218	(0.05,0.4)	R_c	7	3.0×10^{10}	7.4×10^{11}	7.7×10^{11}	4 per cent
3C 236	(0.05,1.4)	r'	6	2.6×10^{11}	6.6×10^{11}	9.2×10^{11}	28 per cent
3C 285	(0.2,0.2)	r'	6	7.2×10^{10}	3.5×10^{11}	4.2×10^{11}	17 per cent
Centaurus A	–	R_T	8	–	1.4×10^{11}	1.4×10^{11}	–
PKS1345+12	(0.05,0.8)	R	11	7.5×10^{10}	8.3×10^{11}	9.0×10^{11}	8 per cent
3C 293	(2.0,0.4)	r'	6	1.6×10^{11}	1.2×10^{11}	2.8×10^{11}	57 per cent
3C 305	(0.4,0.6)	r'	6	1.1×10^{11}	4.3×10^{11}	5.7×10^{11}	19 per cent
3C 321	(0.6,0.2)	r'	6	3.0×10^{10}	5.1×10^{11}	5.4×10^{11}	6 per cent
PKS1549−79	(0.05,0.4)	R	9	5.0×10^9	1.6×10^{11}	1.6×10^{11}	3 per cent
PKS1932−46	–	r'	1	–	3.3×10^{11}	3.3×10^{11}	—
3C 433	(0.05,0.7)	V_{25}	10	3.2×10^{10}	4.3×10^{11}	4.7×10^{11}	7 per cent
PKS2135−209	(0.2,0.2)	i'	1	5.6×10^{10}	3.1×10^{11}	3.7×10^{11}	15 per cent
3C 459	(0.05,0.2)	r'	1	1.3×10^{10}	1.6×10^{11}	1.7×10^{11}	8 per cent

Moreover, our modelling is consistent with young YSP ages for the one other radio galaxy in our sample with a ULIRG-like far-IR luminosity – PKS2135-20 – even if the YSP age in that case cannot be determined with any accuracy, due to the presence of strong nuclear AGN emission.

(iv) *Links with the level of AGN activity.* It is notable that *all* of the objects that have both highly powerful radio emission with $P_{5\,GHz} \geq 10^{26}$ W Hz^{-1} and luminous [O III] line emission with $L_{[O\,III]} \geq 10^{35}$ W[5] have spectra consistent with young YSP ages ($t_{YSP} < 0.1$ Gyr). All seven of these objects (33 per cent of the sample) with powerful jets and luminous AGN are also luminous at far-IR wavelengths ($L_{IR} > 10^{11}$ W). On the other hand, all but one of the objects (NGC 612 is the exception) that have low radio powers with $P_{5\,GHz} < 10^{25}$ W Hz^{-1} have spectra consistent with older, intermediate-age YSP. Thus, there appears to be a link between the level of AGN/jet activity and the age of the YSP, although the relationship is not perfect. Objects that do not fit in with the general trend include 3C 321, which has highly luminous [O III] and far-IR emission but intermediate-age YSP, and 3C 218 which has weak emission lines but much younger YSP. Interestingly both of the latter objects fall off the correlation between radio power and emission-line luminosity: 3C 321 is unusually emission-line luminous for its radio power, whereas 3C 218 has an unusually low emission-line luminosity for its relatively high radio power, perhaps as a consequence of the effect of its rich clus-

ter environment boosting its radio luminosity. We further note that a substantial subset of radio galaxies with quasar-like levels of nuclear activity show no evidence for significant recent star formation activity; these objects are discussed further in Section 5.4.

4.4 Stellar masses

In order to compare the starburst radio galaxies with other types of star-forming galaxies in the local Universe, it is important to consider their stellar masses. We have estimated the total stellar masses by using the monochromatic continuum fluxes derived from the best available total photometric magnitudes to scale the stellar masses derived from our spectral synthesis modelling of the spectra. In each case we used the best-fitting YSP+OSP model to derive the stellar masses for the nuclear spectroscopic aperture, then assumed that the same model was appropriate for the entire stellar halo of the galaxy sampled by the photometric aperture. This assumption is justified on the basis that our spectra show little evidence for major gradients in the stellar populations across the haloes of most of the galaxies in our sample (e.g. Holt et al. 2007). Although the major source of uncertainty in this procedure is likely to be related to the choice of a single stellar model for each galaxy, experiments involving the adoption of extreme models (e.g. assuming that the haloes are dominated by OSPs) suggest that the derived total stellar masses are accurate to within a factor of 2.

The results for the starburst radio galaxies are presented in Table 4 and Fig. 2. They demonstrate that most starburst radio galaxies are giant elliptical galaxies in terms of their total stellar masses.

---

[5] This level of [O III] luminosity corresponds to luminous quasar-like nuclear activity (e.g. Zakamska et al. 2003).
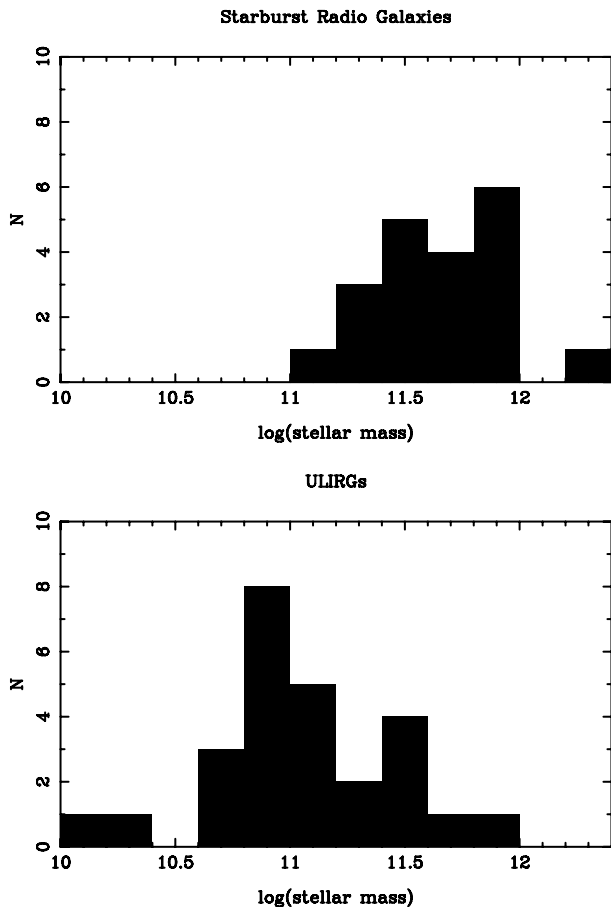
Figure 2. The total stellar masses of starburst radio galaxies (top), compared with those of ULIRGs with $z < 0.13$ from the complete sample (CS) of Rodríguez Zaurín et al. (2009) (bottom). See the text for details of how the masses have been calculated.

Considering the galaxy mass function derived by Cole et al. (2001),[6] the majority of starburst radio galaxies are super-m_*: the mean and median stellar masses are 5.6×10^{11} M$_\odot$ ($4 \times m_*$) and 4.7×10^{11} M$_\odot$ ($3.3 \times m_*$). These results are consistent with those derived for the general population of powerful radio galaxies at all redshifts (e.g. Dunlop et al. 2003; Rocca-Volmerange et al. 2004; Seymour et al. 2007; Inskip et al. 2010). For example, based on the near-IR photometry measurements presented in Inskip et al. (2010), the general population of nearby ($z < 0.5$) 2 Jy radio galaxies has stellar masses in the range $2 \times 10^{11} < M_{\rm stellar} < 2 \times 10^{12}$ M$_\odot$. However, as highlighted in Wills et al. (2008), it is dangerous to generalize, and a minority of radio galaxies have stellar masses that are significantly lower ($\sim m_*$).

Fig. 2 also shows a comparison between the total stellar masses of starburst radio galaxies (top panel) and nearby ULIRGs from the $z < 0.13$ complete sample of Rodríguez Zaurín et al. (2009) (bottom panel), derived using identical techniques. In making this comparison it is important to recognize that the estimated total stellar masses of the ULIRGs have been derived using OSP+YSP models (modelling combination I in Rodríguez Zaurín et al. 2009), which tend to maximize the OSP combination (and hence the total stellar masses), whereas in fact the nuclear spectra of many of ULIRGs can be adequately modelled by combinations of intermediate-age and young

[6] The mass function given in Cole et al. (2001) has a characteristic mass: $m_* = 1.4 \times 10^{11}$ M$_\odot$, adapted to our cosmology.

YSPs, without any contribution from an OSP (combination III in Rodríguez Zaurín et al. 2009), similar to the case of 3C 459 amongst the starburst radio galaxies (Wills et al. 2008). Despite the fact that the masses of ULIRGs in Fig. 2 may be overestimated, most radio galaxies have total stellar masses that are greater than those of most ULIRGs, although there is a significant overlap between the two distributions. Using a K-S two-sample test we can reject the null hypothesis that the two samples have the same mass distributions at the >99.5 per cent level of significance. Overall, this comparison provides a clear demonstration of the fact that, although some radio galaxies *are* ULIRGs and others may have *evolved from* ULIRGs (see Tadhunter et al. 2005), not all ULIRGs can evolve into radio galaxies and vice versa; only the most massive 50 per cent of ULIRG systems are capable of harbouring powerful radio jets. In this context it is notable that, out of the complete sample of 26 $z < 0.13$ ULIRGs investigated by Rodríguez Zaurín et al. (2009), only one is a radio galaxy, and that object – PKS1345+12 (also in our sample of starburst radio galaxies) – has the largest total stellar mass of all the ULIRGs.

5 DISCUSSION

5.1 Triggering radio galaxy activity in galaxy mergers

It is clear that many of the optical morphological features of starburst radio galaxies are consistent with the idea that both the AGN/jet and starburst activity have been triggered as the result of the gas infall associated with galaxy mergers. Hydrodynamical simulations of mergers reveal that they are complex events, and it can take a gigayear or more for the merger remnant to relax and achieve the appearance of a normal galaxy. The main gas infall and star formation are predicted to occur in two major peaks: one at or just after the first pericentre passage of the merging nuclei; the other as the two nuclei finally coalesce (e.g. Mihos & Hernquist 1996). The relative intensity and separation in time of these two peaks depends on several factors such as the morphologies, mass ratios and gas contents of the precursor galaxies, the merger geometries and the importance of feedback processes associated with the AGN and starbursts (Mihos & Hernquist 1996; di Matteo, Springel & Hernquist 2005; di Matteo et al. 2007; Cox et al. 2008; Johansson, Naab & Burkert 2009).

Given that most starburst radio galaxies have massive old stellar populations in addition to their YSP, it is likely that their precursors had significant stellar bulges. Moreover, the relatively large masses and proportional mass contributions of the YSPs (see Table 4) suggest that at least one of the precursors must have been gas rich. In such circumstances the models predict that the second star formation peak – associated with the coalescence of the two nuclei – is likely to be the most intense (Mihos & Hernquist 1996). If the AGN feedback effects are important, and the AGN are triggered concurrently with the starburst, then the star formation will be halted shortly after (<0.1 Gyr) the final coalescence of the nuclei by powerful AGN-induced winds. The time lag between the two star formation peaks is of the order of 0.3–1.5 Gyr, while the major phase of activity associated with the second (more intense) peak is expected to last an order of 0.1 Gyr. However, star formation and AGN activity may not only be associated with the two main peaks of activity, but may also occur – albeit at reduced intensity – at other stages; for example, as the tidal debris rain back down on the merger remnant following the coalescence of the two nuclei. Many of the most recent simulations demonstrate that the fuel supply to the central supermassive black holes can be highly irregular over

Pre–coalescence   Coalescence   Post–coalescence
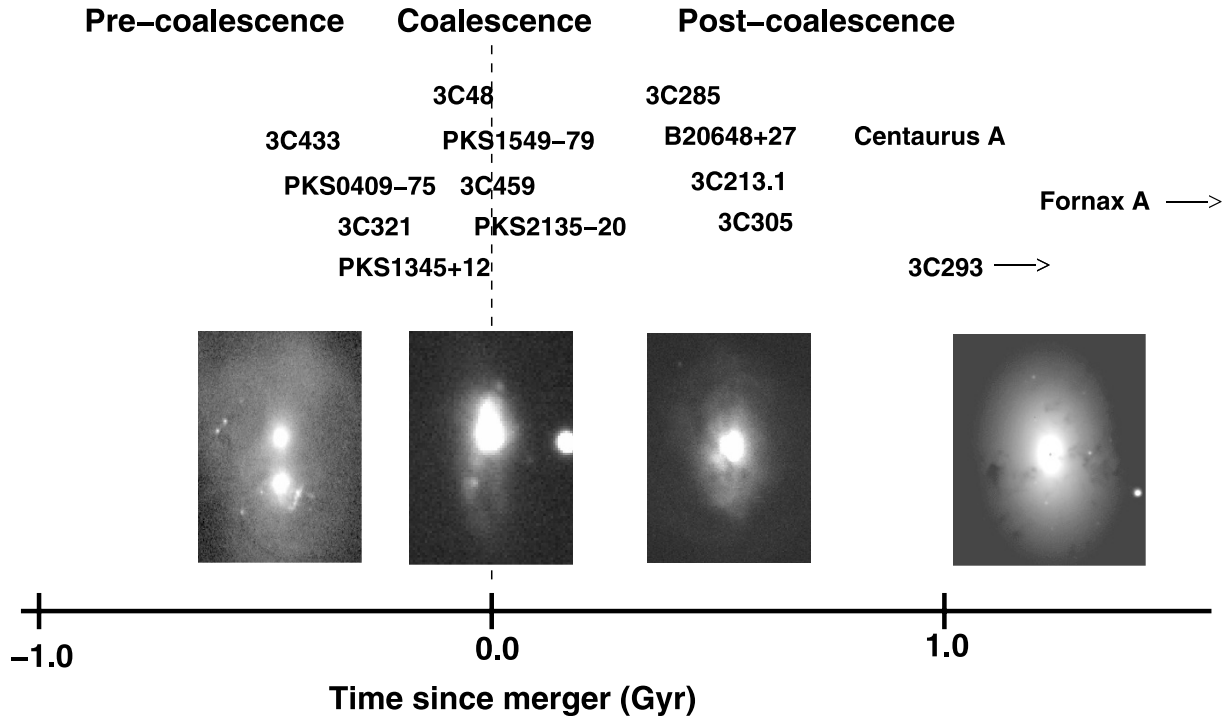
Figure 3. An evolutionary sequence for starburst radio galaxies triggered in galaxy mergers.

the course of a merger (di Matteo et al. 2007; Cox et al. 2008; Johansson et al. 2009).

It is important to emphasize that, as well as the delivery of gas into the *general vicinity* of the supermassive back hole (within $\sim$100 pc – the typical resolution of the hydrodynamical simulations), there may be other time-scales involved in the triggering of the activity. These include the time required for the supermassive black holes from the precursor galaxies to merge, and the time required for the accreted gas to lose sufficient angular momentum to move close enough to the remnant supermassive black hole to fuel the activity (see discussion in Tadhunter et al. 2005). It has also been suggested that the powerful winds associated with the circumnuclear star formation activity may disrupt the flow of gas into the nuclear regions and delay the onset of AGN activity (Davies et al. 2007; Wild et al. 2010). Unfortunately, the current generation of hydrodynamical simulations do not have sufficient resolution to include these processes in any detail. Therefore, in what follows we will assume that the black hole accretion and star formation rates are as (crudely) predicted by the simulations, with the caveat that the reality is likely to be more complex.

We now consider whether, based on their YSP properties and optical morphologies, the objects discussed in this paper are consistent with the merger scenario for the triggering of the activity. Most of the starburst radio galaxies can be fitted into one of the following three categories, each corresponding to a particular phase of a gas-rich merger.[7] This merger sequence is also illustrated in Fig. 3.

(i) *Pre-coalescence.* These double-nucleus systems are observed after the first pericentre passage, but immediately before (within $\sim$0.1 Gyr) the coalescence of the two nuclei, as they move together.

All of these objects have large AGN/jet and far-IR luminosities, reflecting the level of AGN and starburst activity associated with the gas infall expected at this stage of a merger. The YSPs in these systems represent a combination of the younger YSP formed as a consequence of the fresh gas infall associated with coalescence, and intermediate-age stellar populations formed in the first peak of star formation, around the time of the first pericentre passage. The relative importance of the latter two stellar populations will depend on the details of the encounter, and the extent to which the most recent episode of star formation is obscured by dust. Alternatively, any intermediate-age stellar populations could be associated with the captured discs of the precursor galaxies. Examples: PKS0409-75, PKS1345+12, 3C 321 and 3C 433.

(ii) *Coalescence.* These single-nucleus systems are observed in the 0.1 Gyr period immediately following the coalescence of the two nuclei. For major mergers involving gas-rich galaxies with significant bulges, the models predict that this should represent the most active phase of starburst and AGN activity. Due to the fact that the most recent phase of star formation activity has been particularly intense, and is likely to dominate (in flux) over any previous generations of stars, the luminosity-weighted ages in the nuclear regions of these objects are relatively young (<0.1 Gyr). The far-IR, [O III] and radio luminosities are large in this phase, reflecting the high level of AGN and starburst activity associated with the large concentrations of gas and dust in the nuclear regions; in some cases (depending on the details of the merger) the source may attain a ULIRG-like luminosity. Examples: 3C 48[8], PKS1549-79, PKS2135-209 and 3C 459.

---

[7] *Note.* Only objects with good YSP age estimates, that fit clearly in the merger sequence in terms of their ages and morphologies, are included as examples. Misfits are discussed later in this section.

[8] Note that, although it has been proposed that this source contains a secondary nucleus – visible in *HST* images, the putative secondary nucleus is much closer to the primary nucleus (only 1 kpc in projection) than in the cases of the pre-coalescence sources listed above. Therefore, we list it as a coalescence case.

(iii) *Post-coalescence.* These single-nucleus systems still bear the morphological hallmarks of a merger in the recent past (tidal tails, dust lanes, distorted outer isophotes etc.), but they have intermediate-age YSPs ($0.2 < t_{YSP} < 2.5$ Gyr), consistent with them being observed a significant period after the main merger-induced starburst (i.e. the YSPs represent post-starburst stellar populations). This is the scenario outlined in Tadhunter et al. (2005) and Emonts et al. (2006). Unless the AGN/jet activity lasts considerably longer than the 0.1-Gyr maximum lifetime that is typically estimated for powerful extragalactic radio sources (e.g. Leahy, Mulow & Stephens 1989), there must have been a time lag between the main merger-induced starburst and the triggering of the current phase of activity. Examples: B20648+27, 3C 213.1, 3C 285, 3C 293, 3C 305, Centaurus A, Fornax A.

Just as it appears likely that radio-loud AGN activity can be triggered at different stages during a merger, it is also possible that there is more than one episode of AGN/jet activity in the course of a merger. For example, an individual system may undergo a particularly powerful phase of AGN/jet activity as the nuclei coalesce, close to the peak of starburst activity (the coalescence phase above), but the AGN/jet activity may also be triggered (or re-triggered) earlier or later in the merger sequence, depending on the details of the radial gas flows in the merger. Indeed, as noted above, six of the starburst radio galaxies in our sample show evidence for re-triggered radio source activity in the form of high surface brightness inner radio structures and more diffuse and extended outer radio structures (3C 213.1, 3C 218, Cen A, 3C 236, 3C 293, PKS1345+12). Moreover, in the particular case of 3C 236, O'Dea et al. (2001) have argued for multiple phases of jet activity, based on both the double–double morphology of its radio source, and the evidence for two major epochs of star formation in its host galaxy.

We emphasize that not all of the starburst radio galaxies can be readily accommodated within the merger scheme outlined above; there are some prominent misfits. Most notably, the central cluster galaxies 3C 218 and PKS0620-52 do not show clear morphological signs of major mergers, and 3C 218 is also unusual in having relatively young YSP ($t_{YSP} \sim 0.05$ Gyr) but low emission line and far-IR luminosities (the age of the YSP in PKS0620-52 is not well determined). PKS0023-26 may also represent an ambiguous case in the sense that it lies at the heart of a rich cluster of galaxies, and has a peculiar amorphous outer envelope that is difficult to classify in terms of the merger sequence (although a merger cannot be entirely ruled out).

In the case of the one system in our sample that shows evidence for large-scale, and relatively settled, gaseous disc – NGC 612 – it is not clear whether the AGN/jet activity has been triggered by interactions with massive galaxies on a large scale in the wider galaxy group (as may be evidenced by the H I observations), or by recent mergers/interactions with closer companion galaxies (see Emonts et al. 2008a). The latter seems more likely given that NGC 612 shows an optical shell structure, along with YSPs that are much younger ($t_{YSP} < 0.1$ Gyr) than the estimated time since its closest approach to the massive companion galaxy NGC 619 (≥ 1 Gyr). Clearly, the possibility of multiple interactions and mergers in galaxy groups can complicate the interpretation of the galaxy morphologies and YSP ages in terms of a simple merger sequence.

Finally we note that, while the properties of the most luminous starburst radio galaxies – in particular, the ULIRG-like coalescence systems – are consistent with triggering in major (similar mass) gas-rich mergers, it is difficult to rule out minor mergers as the trigger for some of the other systems. Indeed, it has been argued

that the large-scale features of Centaurus A are consistent with a minor (1:10) merger between the host radio galaxy and a smaller disc galaxy (Malin, Quinn & Graham 1983).

5.2 Do cooling flows play a significant role?

As noted in the previous section, some of the starburst radio galaxies that are situated close to the centres of rich clusters of galaxies are not readily accommodated in the merger sequence. For such objects cooling flows[9] associated with the hot X-ray-emitting gas may provide an alternative triggering mechanism for both the visible star formation and the AGN/jet activity. This mechanism is supported by the irregular morphologies and kinematics of the emission-line gas in central cluster galaxies hosting radio sources (Tadhunter et al. 1989; Baum et al. 1992). Moreover, while the high velocity dispersions of the galaxies in the centres of massive galaxy clusters can hamper gas accretion via major, gas-rich mergers, there is no such problem for the accretion of warm/hot gas via cooling flows, since the cooling gas will naturally fall towards the centre of the cluster potential well.

Although star formation has been discussed as a potential sink for the cooling gas, until recently the apparently large differences between the estimated hot-gas cooling rates and the star formation rates in the central cluster galaxies suggested that only a small fraction of the cooling gas ends up forming stars (e.g. McNamara & O'Connell 1989). However, spectroscopic observations with the new generation of X-ray satellites have led to a major downward revision in estimates of the hot-gas cooling rates, so that they are now much closer to the star formation rates. Therefore, it is plausible that a significant fraction of the cooling gas does in fact form stars (see Rafferty et al. 2006). In the cases of the three cooling flow candidates in our sample, based on their infrared luminosities and the relation of Kennicutt (1998), the star formation rates are 5, 4 and 25 M$_\odot$ yr^{-1} for PKS0620-52, 3C 218(Hydra A) and PKS0023-36, respectively. Of these three, only 3C 218 has published high-quality X-ray observations, and its hot-gas cooling rate of 16 ± 4 M$_\odot$ yr^{-1} (Rafferty et al. 2006) proves to be within a factor of 4 of the star formation rate.

Given the agreement between its star formation and hot-gas cooling rates, 3C 218 is one of the best candidates for an object in which the activity has been triggered by the warm/cool gas condensing out of a cooling flow. However, even in the case of 3C 218 we cannot entirely rule out the idea that the activity has been triggered in a galaxy merger or interaction, since it is possible for central cluster galaxies to undergo mergers that could, potentially, form star-forming gaseous discs similar to that associated with the dust lane in the central regions of 3C 218 (Ramos Almeida et al. 2010a). Although such discs (and the merging galaxies that produced them) may represent only a small fraction of the total masses of the cD galaxies, the associated gas infall rates may be sufficient to fuel the AGN/jet activity in the nuclei on the requisite time-scales. Note that the large-scale morphological signatures of galaxy mergers (e.g. tidal tails, fans, shells) are more difficult to detect against the light of the massive stellar haloes of the central cluster galaxies than they are in lower-mass elliptical galaxies; the tidal features are also

---

[9] By cooling flows we mean here the cooling of the large-scale hot ($\sim 10^7$–10^8 K) X-ray-emitting gas of the cluster to cooler phases of the ISM in the central cluster galaxy, where it can form stars and/or be accreted by the central black holes. The direct accretion of the hot gas itself by the central black hole will be discussed in the following section.

likely to be erased on a relatively short time-scale by ongoing tidal interactions between all the galaxies in the dense central regions of the galaxy clusters.

5.3 Triggering the activity in weak-line radio galaxies

As a class, low-power FRI radio galaxies are almost invariably classified as weak-line radio galaxies (WLRG) at optical wavelengths. However, a significant proportion of FRII galaxies also have WLRG spectra, with [O III]λ5007 and mid-IR luminosities that are an order of magnitude lower than narrow- and broad-line radio galaxies (NLRG/BLRG) of comparable radio power (Tadhunter et al. 1998; Dicken et al. 2009). On the basis of their nuclear X-ray and emission line properties, and the way that their emission-line luminosities and absolute magnitudes correlate with radio power, it has been suggested that the nuclear accretion rate or accretion mode in WLRG is distinct from that in their strong-lined radio galaxy counterparts (e.g. Hardcastle et al. 2007; Buttiglione et al. 2010). In particular, it has been argued that WLRG represent objects in which the AGN/jet activity is fuelled via Bondi accretion of the hot X-ray-emitting ISM, while strong-lined radio galaxies represent objects in which the activity is fuelled by the accretion cooler phases of the ISM. For low-power radio galaxies the Bondi accretion hypothesis is supported by correlations between galaxy/black hole mass and the fraction of galaxies that are radio-loud, the relatively large proportion of galaxies that are radio-loud at large galaxy/black hole mass (suggesting a high duty cycle) and the fact that the energy input of radio jets fuelled by Bondi accretion is sufficient to balance radiative losses of the hot X-ray-emitting haloes of the host giant elliptical galaxies (Best et al. 2005; Allen et al. 2006; Best et al. 2006).

Significant star formation is not expected in the case of triggering via Bondi accretion of the hot ISM. Therefore, it is interesting that a significant subset of the starburst radio galaxies are classed WLRG (NGC 612, PKS0620-52, 3C 213.1, 3C 218, 3C 236, 3C 293, Fornax A, Centaurus A). Although some of such objects (PKS0620-52, 3C 218) are candidates for fuelling via cooling flows (see Section 5.2 above), more than 50 per cent of the WLRG in our sample of starburst radio galaxies can be classified as post-coalescence or late post-coalescence systems, with evidence for a rich ISM in the circumnuclear regions in the form of circumnuclear dust lanes, as well as other signs that they have been involved in mergers in the recent past. This suggests a possible alternative to fuelling via Bondi accretion of the hot ISM: accretion of the cool ISM at a slow rate from the debris discs of galaxy mergers. As the discs settle it is expected that the shocks associated with the gaseous dissipation process will lead to a net infall of gas, and also produce a LINER-type emission line spectrum, similar to those observed in WLRG (Dopita et al. 1997).

In the later post-merger stages the debris discs may also act as large reservoirs of *potential* fuel for the AGN/jet activity, but external stimuli, such as interactions with neighbouring galaxies or the accretion of satellite galaxies, may be required to perturb the discs and induce radial gas infalls that are sufficient to trigger the AGN. This might help to explain late post-coalescence systems such as the iconic FRI radio galaxies Centaurus A and Fornax A, which appear to have been triggered a substantial period after (∼2–3 Gyr after in the case of Fornax A) the mergers associated with the formation of the dust lanes. In such cases, the original merger may not have triggered the current phase of nuclear activity directly, but rather delivered a reservoir of cool gas that was then perturbed by more minor galaxy interactions to produce the observed level of

activity. In this context it is notable that Centaurus A shows evidence for an ongoing satellite galaxy accretion event in the form of a blue tidal stream (Peng et al. 2002).

Overall, the assumption that *all* WLRG are fuelled by Bondi accretion of the hot ISM is likely to represent an oversimplification; for a significant fraction – including some FRI radio galaxies – slow accretion of cooler gas from the debris discs of galaxy mergers represents a viable alternative mechanism. This is consistent with the X-ray and mid-IR evidence for compact, cool dust/gas structures in the nuclear regions of a minority of WLRG, including Centaurus A (Evans et al. 2004; Ramos Almeida et al. 2010a).

5.4 Non-starburst radio galaxies

The discussion above has concentrated on starburst radio galaxies that show strong evidence for recent star formation activity at optical wavelengths. However, such objects comprise only a small proportion (∼15–25 per cent) of the full population of powerful radio-loud AGN in the local Universe. Clearly, it is important to consider how the AGN/jet activity is triggered in the 75–85 per cent majority of powerful radio galaxies that do not show strong signs of optical star formation activity. Note that many of the latter belong to the class of strong-lined FRII radio sources in which the AGN/jet activity is generally considered to be triggered by accretion of the cooler phases of the ISM (Hardcastle et al. 2007; Buttiglione et al. 2010).

One possibility is that the non-starburst radio galaxies are objects in which the AGN/jet activity has been triggered or re-triggered in the late post-coalescence phase, >1 Gyr after the starburst associated with the coalescence of the nuclei in the merger. As argued in Wills et al. (2002), after ∼1 Gyr it can be difficult to detect a merger-induced starburst at optical wavelengths against the light of the giant elliptical galaxy host, especially if the YSP comprises a relatively small fraction of the total stellar mass and/or suffers a moderate amount of extinction. In the late post-coalescence phase, the morphological signs of mergers also become more difficult to detect, especially for radio galaxies at intermediate/high redshifts. The main problem with this explanation is that, for strong-lined, non-starburst FRII radio galaxies, the moderate rates of gas infall associated with the debris discs may not be sufficient to fuel the prodigious nuclear activity. Indeed, many of the starburst radio galaxies that we identified above as post-coalescence systems are WLRG.

Alternatively, it is possible that the activity in the non-starburst radio galaxies has been triggered by close encounters with gas-rich companion galaxies, or following the first pericentre passages of the merging nuclei in galaxy mergers. In the latter case, hydrodynamical simulations show that the tidal forces following the first encounter induce significant radial infalls of gas into the nuclei for an extended period (∼0.5–1.0 Gyr: Springel, di Matteo & Hernquist 2005; Johansson et al. 2009) around the time of closest approach. Such infalls may be capable of fuelling the prodigious AGN/jet activity in strong-lined radio galaxies. However, in cases in which the merging nuclei have significant bulges (highly likely in the case of radio galaxies), only a relatively low level of star formation is expected at this stage. This mechanism may be supported by the finding of a relatively high incidence of tidal bridge features and tidally distorted companion galaxies in deep imaging observations of non-starburst radio galaxies in the 2 Jy sample (Ramos Almeida et al. 2010a); it is further supported by detailed studies of individual radio galaxies in interacting groups (Inskip et al. 2007, 2008).

A final possibility is that non-starburst radio galaxies are triggered in relatively minor mergers (1:3 or less), or in major mergers that are relatively gas poor ('dry'). In such cases relatively low levels of star formation are expected, which are likely to be difficult to detect against the light of the old stellar populations in the host galaxies. However, without further theoretical work, it is not clear whether minor or gas-poor mergers would be capable of delivering sufficient gas to the nuclear regions to fuel the quasar-like levels of nuclear activity detected in some non-starburst radio galaxies.

5.5 The radio structures of starburst radio galaxies

An interesting aspect of starburst radio galaxies is that they show a high incidence of unusual radio structures: our sample includes several compact CSS/GPS sources, as well as sources with relatively bright steep spectrum core structures, diffuse outer haloes and double–double structures. What (if any) is the relationship between these unusual radio structures and the presence of young stellar populations in the host galaxies?

As already discussed above, double–double sources, and sources with compact high surface brightness inner structures combined with diffuse outer haloes, may represent cases in which the radio jet activity has been re-triggered (but see Morganti et al. 1999 and Wise et al. 2007 for counter-arguments in the cases of Centaurus A and Hydra A). Given the complexity of the gas infall histories of major gas-rich mergers, it is certainly plausible that each merging system undergoes more than one phase of AGN/jet activity, thus explaining the presence of such sources in our sample.

Considering the compact (CSS/GPS) radio sources, there is direct observational evidence from measurements of hotspot advance speeds that CSS/GPS radio sources are relatively youthful (10^4–10^6 yr). However, since the CSS/GPS radio sources are generally estimated to be much younger than the YSPs detected in their host galaxies ($t_{YSP} \sim 10^7$–10^9 yr), the youth of the compact sources does not necessarily help to explain their relatively high rate of occurrence in our sample of starburst radio galaxies.

Alternatively, the high incidence of CSS/GPS sources in the starburst radio galaxies sample may be the consequence of an observational selection effect as follows. We expect a relatively rich and dense ISM to be present in the nuclear regions of merging systems, especially around the time of nuclear coalescence. A radio source triggered in a merger will interact particularly strongly with this rich ISM in the early stages of the radio source history, as the jets expand through the central regions of the host galaxies; direct evidence for strong jet–cloud interactions in young radio sources is provided by their extreme emission-line kinematics (Holt, Tadhunter & Morganti 2008). The strong interactions between the jets and the rich ISM associated with the mergers will not only result in extreme emission line kinematics, but may also affect the conversion of jet power into radio luminosity, boosting the radio luminosities of sources. There is already evidence that interaction with the relatively dense, hot X-ray haloes associated with clusters of galaxies boosts the radio luminosities of jets for a given jet power (Barthel & Arnaud 1996), and it is plausible that there will be a similar boosting effect when the jets strongly interact with the (cooler) ISM in the central regions of merger remnants. Indeed, strong enhancements in the radio emission are observed at the sites of interactions between radio jets and warm emission line clouds in the haloes of radio galaxies in the local Universe (e.g. van Breugel et al. 1985, 1986; Fosbury et al. 1998; Tadhunter et al. 2000). For a given intrinsic jet power, this flux-boosting will lead to the compact radio sources that are triggered in young, star-forming merger

remnants being preferentially selected in flux-limited radio surveys. This in turn could explain the relatively high rate of occurrence of compact radio sources amongst the starburst radio galaxies, as well as the bias of the compact sources towards relatively young YSP ages ($t_{YSP} < 0.1$ Gyr; see Section 4.1).

The interaction of the jets with the richer gaseous environments present in merger remnants could also help to explain the relatively high incidence of extended radio sources with compact steep spectrum cores in our sample, since such interactions have the potential to boost the radio emission from the jets, even if the radio lobes are well outside the central regions of the galaxies.

6 CONCLUSIONS AND FUTURE WORK

In this paper we have discussed the properties of the YSPs in the ~15–25 per cent of powerful radio galaxies that show strong evidence for recent star formation activity at optical wavelengths. Combined with information about the morphologies of the host galaxies, the YSP properties of most of these starburst radio galaxies are consistent with the triggering of both starburst and AGN/jet activity in galaxy mergers in which at least one of the merging galaxies is gas rich. However, the triggering of the AGN/jet activity is not confined to a single evolutionary phase of galaxy mergers. While in a significant subset of objects the AGN/jet activity has been triggered within 0.1 Gyr of the coalescence of merging nuclei, close to the expected peaks of the merger-induced starbursts, many objects are observed in the post-coalescence phase, >0.2 Gyr after the starburst peaks. In the former group the triggering of the activity can be readily identified with the major infalls of gas that are predicted to occur around the time of coalescence. On the other hand, in the latter group the nature of the link between the triggering of the AGN/jet and the original starburst-inducing mergers is less clear: late-time infall of merger debris, settling of the debris discs to an equilibrium configuration and perturbation of the debris discs by minor mergers and encounters, are all possibilities for the triggering of the activity in these, generally lower luminosity, objects.

Our results clearly demonstrate that luminous radio-loud AGN *can* be triggered close to the peaks of major gas-rich mergers. However, the relatively low incidence of radio-loud AGN in nearby ULIRGs suggests that, even under similar conditions of gas infall, it is not inevitable that radio-loud AGN activity *will* be triggered in such mergers. Indeed our comparison of the stellar masses of ULIRGs and starburst radio galaxies suggests that the triggering of powerful radio-loud AGN activity is most likely to occur in the most massive merger remnants, consistent with other studies of AGN host galaxies that provide evidence for a link between host galaxy mass (and hence black hole mass) and the incidence of the radio-loud AGN population (e.g. Lacy et al. 2001).

Overall, if we also take into consideration the evidence that some radio-loud AGN are triggered by the accretion of gas from the hot X-ray haloes, either via cooling flows or the direct (Bondi) accretion of hot gas, it appears unlikely that radio-loudness is solely a consequence of a particular mechanism for the delivering of the fuel supply to the nuclear regions. Rather, the ability to produce powerful relativistic jets is more likely to be related to the intrinsic properties of energy-generating regions (e.g. the spin and/or mass of the supermassive black hole).

Finally, we emphasize that a considerable fraction of powerful radio galaxies (~75–85 per cent) do not show evidence for energetically significant starburst activity at either optical or MFIR wavelengths. Therefore, in order to complete our understanding of triggering of the activity in radio-loud AGN, in the future it will be

important to compare the host galaxy properties and environments of the non-starburst majority of radio galaxies, with those of the starburst minority discussed in this paper.

REFERENCES

Allen S. W., Dunn R. J. H., Fabian A. C., Taylor G. B., Reynolds C. S., 2006, MNRAS, 372, 21
Aretxaga I., Terlevich E., Terlevich R., Cotter G., Diaz A. I., 2001, MNRAS, 325, 636
Baldi R. D., Capetti A., 2008, A&A, 489, 989
Barnes J. E., 2004, MNRAS, 350, 798
Barthel P. D., Arnaud K. A., 1996, MNRAS, 283, L45
Batcheldor D., Tadhunter C., Holt J., Morganti R., O'Dea C. P., Axon D. J., Koekemoer A., 2007, ApJ, 661, 70
Baum S. A., Heckman T. M., van Breugel W., 1992, ApJ, 398, 208
Bennert N., Canalizo G., Jungwiert B., Stockton A., Schweizer F., Peng C. Y., Lacy M., 2008, ApJ, 677, 846
Benson A. J., Bower R. G., Frenk C. S., Lacey C. G., Baugh J. L., Cole S., 2003, ApJ, 599, 38
Best P. N., Kauffmann G., Heckman T. M., Brinchmann J., Charlot S., Ivezic. Z., White S. D. M., 2005, MNRAS, 362, 25
Best P. N., Kaiser C. R., Heckman T. M., Kauffmann G., 2006, MNRAS, 368, L67
Bower R. G., Benson A. J., Malbon R., Helly J. C., Frenk C. S., Baugh C. M., Cole S., Lacey C. G., 2006, MNRAS, 370, 645
Boyce P. J., Disney M. J., Bleaken D. G., 1999, MNRAS, 302, 39
Bremer M. N., Fabian A. C., Crawford C. S., 1997, MNRAS, 284, 213
Brotherton M. S. et al., 1999, ApJ, 520, L87
Bruzual G., Charlot S., 2003, A&A, 409, 511
Buttiglione S., Capetti A., Celotti A., Axon D. J., Chiaberge M., Macchetto F., Sparks W. B., 2010, A&A, 509, 6
Canalizo G., Stockton A., 2000, ApJ, 528, 201
Canalizo G., Bennert N., Jungwiert B., Stockton A., Schweizer F., Lacy M., Peng C., 2007, ApJ, 669, 801
Cattaneo A., et al., 2009, Nat, 460, 213
Cole C. et al., 2001, MNRAS, 326, 255
Cox T. J., Jonsson P., Somerville R. S., Primack J. R., Dekel A., 2008, MNRAS, 384, 386
Croft S. et al., 2006, ApJ, 647, 1040
Davies R. I., Sánchez F., Mueller F., Genzel R., Tacconi L. J., Hicks E. K. S., Friedrich S., Sternberg A., 2007, ApJ, 671, 1388
de Koff S., Baum S. A., Sparks W. B., Biretta J., Golombek D., Macchetto F., McCarthy P., Miley G. K., 1996, ApJS, 107, 621
de Koff S. et al., 2000, ApJS, 129, 33
di Matteo T., Springel V., Hernquist L., 2005, Nat, 433, 604
di Matteo P., Combes F., Melchior A.-L., Semelin B., 2007, A&A, 468, 61
Dicken D., Tadhunter C., Morganti R., Buchanan C., Oosterloo T., Axon D., 2008, ApJ, 678, 712
Dicken D., Tadhunter C., Axon D., Morganti R., Inskip K. J., Holt J., González Delgado R., Groves B., 2009, ApJ, 694, 268
Dicken D., Tadhunter C., Axon D., Robinson A., Morganti R., Kharb P., 2010, ApJ, 722, 1333

Dopita M. A., Koratkar A. P., Allen M. G., Tsvetanov Z. I., Ford H. C., Bibknell G. V., Sutherland R. S., 1997, ApJ, 490, 202
Drake C. L., McGregor P. J., Dopita M. A., 2004, AJ, 128, 955
Dunlop J. S., Peacock J. A., 1990, MNRAS, 247, 19
Dunlop J. S., McClure R. J., Kukula M. J., Baum S. A., O'Dea C. P., Hughes D. H., 2003, MNRAS, 340, 1095
Emonts B. H. C., Morganti R., Tadhunter C. N., Oosterloo T. A., Holt J., van der Hulst J. M., 2005, MNRAS, 362, 931
Emonts B. H. C., Morganti R., Tadhunter C. N., Holt J., Oosterloo T. A., van der Hulst J. M., Wills K. A., 2006, A&A, 454, 125
Emonts B. H. C., Morganti R., Oosterloo T. A., Holt J., Tadhunter C. N., van der Hulst J. M., Ojha R., Sadler E. M., 2008a, MNRAS, 387, 197
Emonts B. H. C., Morganti R., van Gorkom J. H., Oosterloo T. A., Brogt E., Tadhunter C. N., 2008b, A&A, 488, 519
Evans D. A., Kraft R. P., Worrall D. M., Hardcastle M. J., Jones C., Forman W. R., Murray S. S., 2004, ApJ, 612, 786
Evans D. A. et al., 2008, ApJ, 675, 1057
Fabian A. C., 1999, MNRAS, 308, L39
Fosbury R. A. E., Morganti R., Wilson W., Ekers R. D., di Serego Aligieri S., Tadhunter C. N., 1998, MNRAS, 296, 701
González-Serrano J. I., Carballo R., 2000, A&AS, 142, 353
Goudfrooij P., Mack J., Kissler-Patig M., Meylan G., Minniti D., 2001, MNRAS, 322, 643
Govoni F., Feretti L., Giovannini G., 2000, A&AS, 353, 507
Hardcastle M. J., Evans D. A., Croston J. H., 2007, MNRAS, 376, 1849
Heckman T. M., Miley G. K., Balick B., van Bruegel W. J. M., Butcher H. R., 1982, ApJ, 262, 529
Heckman T. M., Smith E. P., Baum S. A., van Bruegel W., Miley G. K., Illingworth G. D., Bothun G. D., Balick B., 1986, ApJ, 311, 526
Holt J., Tadhunter C. N., Morganti R., 2003, MNRAS, 342, 227
Holt J., Tadhunter C. N., Morganti R., Bellamy M., González Delgado R. M., Tzioumis A., Inskip K. J., 2006, MNRAS, 370, 1633
Holt J., Tadhunter C. N., González Delgado R. M., Inskip K. J., Rodríguez Zaurín J., Emonts B. H. C., Morganti R., Wills K. A., 2007, MNRAS, 381, 611
Holt J., Tadhunter C. N., Morganti R., 2008, MNRAS, 387, 639
Inskip K. J., Tadhunter C. N., Dicken D., Holt J., Villar-Martín M., Morganti R., 2007, MNRAS, 382, 95
Inskip K. J, Villar-Martín M., Tadhunter C. N., Morganti R., Holt J., Dicken D., 2008, MNRAS, 386, 1797
Inskip K. J., Tadhunter C. N., Morganti R., Holt J., Ramos Almeida C., Dicken D., 2010, MNRAS, 407, 1739
Israel F. P., 1998, A&ARv, 8, 237
Johansson P. H., Naab T., Burkert A., 2009, ApJ, 690, 802
Kennicutt R. C., 1998, ApJ, 498, 541
Kim D.-C., Veilleux S., Sanders D. B., 2002, ApJS, 143, 277
Kuntschner H., 2000, MNRAS, 315, 184
Lacy M., Laurent-Muehleisen S. A., Ridgway S. E., Becker R. H., White R. L., 2001, ApJ, 551, L17
Lauberts A., Valentijn E. A., 1989, The Surface Photometry Catalogues of the ESO-Uppsala Galaxies, Garching bei Munchen, European Southern Observatory
Leahy J. P., Muxlow T. W. B., Stephens P. W., 1989, MNRAS, 239, 401
Madau P., Ferguson H. C., Dickinson M. E., Giavalisco M., Steidel C. C., Fruchter A., 1996, MNRAS, 283, 1388
Malin D. F., Carter D., 1983, ApJ, 274, 534
Malin D. F., Quinn P. J., Graham J. A., 1983, ApJ, 272, L5
McNamara B. R., O'Connell R. W., 1989, AJ, 98, 2018
Melnick J., Gopal-Krishna , Terlevich R., 1997, A&A, 318, 337
Mihos C. J., Hernquist L., 1996, 464, 641
Morganti, R., Killeen N. E. B., Ekers R. D., Oosterloo T. A., 1999, MNRAS, 307, 750
Morganti R., Oosterloo T. A., Emonts B. H., van der Hulst J. M., Tadhunter C. N., 2003, ApJ, 593, L69
Morganti R., Oosterloo T. A., tadhunter C. N., van Moorsel G., Emonts B., 2005, A&A, 439, 521
O'Dea C. P., Koekemoer A. M., Baum S. A., Sparks W. B., Martel A. R., Allen M. G., Macchetto F. D., 2001, AJ, 121, 1915

Peng E. W., Ford H. C., Freeman K., White R. L., 2002, AJ, 124, 3144
Peng E. W., Ford H. C., Freeman K. C., 2004, ApJ, 602, 705
Persson S. E., Frogel J. A., Aaronson M., 1979, ApJS, 39, 61
Quillen A. C., Graham J. R., Frogel J. A., 1993, ApJ, 412, 550
Rafferty D. A., McNamara B. R., Nulsen P. E. L., Wise M. W., 2006, ApJ, 652, 216
Raimann D., Storchi-Bergmann T., Quintana H., Hunstead R., Wisotski L., 2005, MNRAS, 364, 1239
Ramos Almeida C., Tadhunter C. N., Inskip K. J., Morganti R., 2010a, MNRAS, in press
Ramos Almeida C., Dicken D., Tadhunter C. N., Asensio Ramos A., Inskip K. J., Hardcastle M. J., Mingo B., 2010b, MNRAS, submitted
Rocca-Volmerange B., le Borgne D., de Breuck C., Fioc M., Moy E., 2004, A&A, 415, 931
Rodríguez Zaurín J., Holt J., Tadhunter C. N., González Delgado R. M., 2007, MNRAS, 375, 1133
Rodríguez-Zaurín J., Tadhunter C. N., González-Delgado R. M., 2009, MNRAS, 400, 1139
Rodríguez-Zaurín J., Tadhunter C. N., González-Delgado R. M., 2010, MNRAS, 403, 1317
Sanders D. B., Mirabel I. F., 1996, ARA&A, 34, 749
Schiminovich D., van Gorkom J. H., van der Hulst J. M., Kasow S., 1994, ApJ, 423, L101
Schlegel D. J., Finkbeiner D. P., Davis M., 1998, ApJ, 500, 525
Seaton M. J., 1979, MNRAS, 187, 785
Seymour N. et al., 2007, ApJS, 171, 353
Siebert J., Brinkmann W., Morganti R., Tadhunter C. N., Danziger I. J., Fosbury R. A. E., di Serego Alighieri S., 1996, MNRAS, 279, 1331
Silk J., Rees M. J., 1998, A&A, 331, L1
Smith E. P., Heckman T. P., 1989, ApJ, 341, 658
Sparke L. S., 1996, ApJ, 473, 810
Springel V., di Matteo T., Hernquist L., 2005, MNRAS, 361, 776
Stanghellini C., O'Dea C. P. O., Dallacasa D., cassaro P., Baum S. A., Fanti R., Fanti C., 2005, A&A, 443, 891
Stockton A., Canalizo G., Fu H., Keel W., 2007, ApJ, 659, 195
Tadhunter C. N., Fosbury R. A. E., Quinn P. J., 1989, MNRAS, 240, 225
Tadhunter C. N., Dickson R. C., Shaw M. A., 1996, MNRAS, 281, 591
Tadhunter C. N., Morganti R., Robinson A., Dickson R., Villar-Martin M., Fosbury R. A. E., 1998, MNRAS, 298, 1035
Tadhunter C. N., Villar-Martin M., Morganti R., Bland-Hawthorn J., Axon D., 2000, MNRAS, 314, 849
Tadhunter C., Wills K., Morganti R., Oosterloo T., Dickson R., 2001, MNRAS, 327, 227
Tadhunter C. N., Dickson R., Morganti R., Robinson T. G., Wills K., Villar-Martín M., Hughes M., 2002, MNRAS, 330, 977
Tadhunter C. N., Robinson T. G., González Delgado R. M., Wills K., Morganti R., 2005, MNRAS, 356, 480
Tadhunter C. et al., 2007, ApJ, 661, L13
Thomasson P., Saikia D. J., Muxlow T. W. B., 2003, MNRAS, 341, 91
Trussoni E., Vagnetti F., Massaglia S., Feretti L., Parma P., Morganti R., Fanti R., Padovani P., 1999, A&A, 348, 437
Tzioumis A. et al., 2002, A&A, 392, 841
van Bruegel W. J. M., Dey A., 1993, ApJ, 414, 563
van Breugel W., Balick B., Heckman T., Miley G., Helfland D., 1983, AJ, 88, 40
van Breugel W., Miley G., Heckman T., Butcher H., Bridle A., 1985, ApJ, 290, 496
van Breugel W., Heckman T., Miley G., Filippenko A. V., 1986, ApJ, 311, 58
Villar-Martín M., Tadhunter C., Morganti R., Clark N., Killeen N., Axon D., 1998, A&A, 332, 479
Villar-Martín M., Tadhunter C. N., Morganti R., Holt J., 2005, MNRAS, 359, L5
Wild V., Heckman T., Charlot S., 2010, MNRAS, 405, 933
Wilkinson P. N., Tzioumis A. K., Benson J. M., Walker R. C., Simon R. S., Kahn F. D., 1991, Nat, 352, 313
Wills K. A., Tadhunter C. N., Robinson T. G., Morganti R., 2002, MNRAS, 333, 211
Wills K. A., Morganti R., Tadhunter C. N., Robnson T. G., Villar-Martín M., 2004, MNRAS, 347, 771
Wills K. A., Tadhunter C., Holt J., González Delgado R., Inskip K. J., Rodríguez Zaurín J., Morganti R., 2008, MNRAS, 385, 136
Wise M. W., McNamara B. R., Nulsen P. E. J., Houck J. C., David L. P., 2007, ApJ, 659, 1153
Zakamska N. L. et al., 2003, AJ, 126, 2125

APPENDIX A: DESCRIPTIONS OF INDIVIDUAL OBJECTS

A0.1 PKS0023-26

Fig. A1 presents a Gemini r'-band image for the host galaxy of this compact steep spectrum radio source ($D = 2.9$ kpc: Tzioumis et al. 2002) taken from Ramos Almeida et al. (2010a). This re-
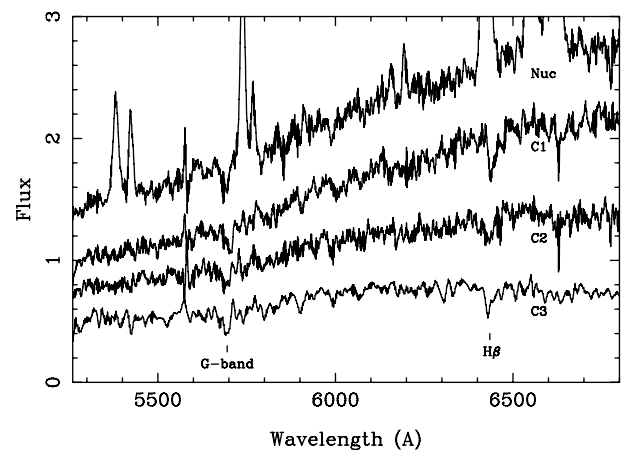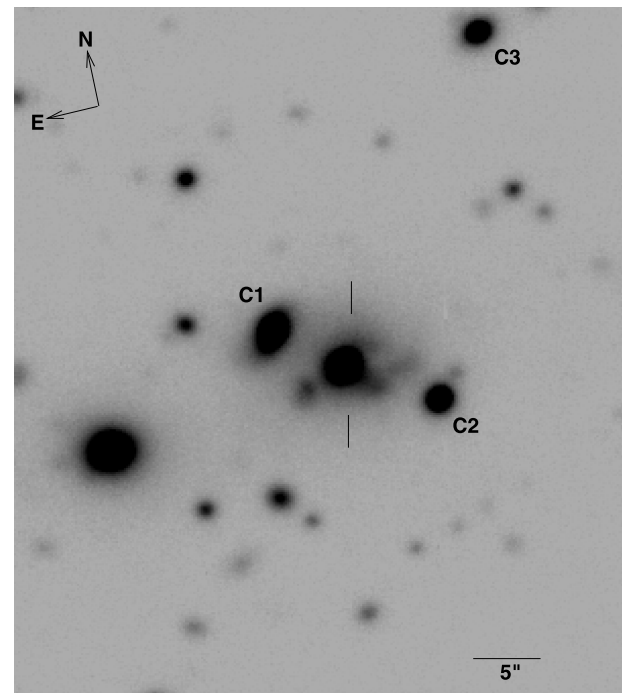
Figure A1. Image and spectra for PKS0023-26 and companion galaxies. Top: r'-band Gemini image with companion galaxies labelled (the radio source host galaxy is at the centre of the field). Bottom: VLT spectra of PKS0023-26 and the three companion galaxies, showing the clear detection of Hβ and the G-band features in the spectra of the companions.

veals that it shares a common envelope with two early-type galaxies at projected distances of 5.8 arcsec (26 kpc) to the NE (C1) and 6.9 arcsec (31 kpc) to the SW (C2). Analysis of our VLT/FORS spectrum along PA51 demonstrates that the companion galaxies have a similar redshift to PKS0023-26 ($z_{\rm nuc} = 0.321955 \pm 0.000014$), as does a further early-type galaxy 25.8 arcsec (116 kpc) to the NW (C3), which falls within the slit for our PA145 VLT/FORS1 spectra. Based on measurements of the detected Hβ absorption features, the redshifts of C1, C2 and C3 are $z_{C1} = 0.32499 \pm 0.00015$, $z_{C2} = 0.32282 \pm 0.00033$ and $z_{C3} = 0.32318 \pm 0.00028$, corresponding to velocity shifts relative to the rest frame of the nucleus of PKS0023-26 of $+690 \pm 34$, $+200 \pm 75$ and $+280 \pm 60$ km s^{-1}, respectively. In fact, the field shows several early-type galaxies close (in projection) to PKS0023-26, suggesting that it lies at the heart of a rich cluster of galaxies. However, perhaps the most interesting feature of the image is the extraordinary amorphous structure that lies between PKS0023-26 and its two closest companions. This appears to be crossed by dust lanes, and may comprise regions of active star formation within the extended halo of the galaxy. Although the halo structure is too faint to study in detail with our existing spectroscopic observations, our deep spectrum of the brighter core of the galaxy reveals a YSP with a relatively young age (<0.05 Gyr: Holt et al. 2007). Further evidence for recent star formation is provided by the fact that PKS0023-26 is significantly brighter at 70 and 160 μm than most other radio galaxies in the 2 Jy sample of similar [O III]λ5007 emission-line luminosity, and also shows relatively cool MFIR colours (Dicken et al. 2009).

A0.2 NGC 612

This nearby source is one of the few powerful radio galaxies to be unambiguously classified as an S0 galaxy based on its optical morphology. Close to the FRI/FRII borderline in terms of its radio luminosity, its radio morphology shows correspondingly hybrid characteristics. As discussed in detail in (Emonts et al. 2008a), the dust lane associated with the optical disc of this galaxy is warped, and there are signs of faint shell structures in its outer envelope, suggestive of a past galaxy interaction. In this context it is notable that 21-cm radio observations reveal an extended H I gas structure ($D > 160$ kpc), that appears to connect NGC 612 with two faint companion galaxies; they also reveal that NGC 612 is connected by an H I bridge to a gas-rich companion galaxy ~400 kpc to the east (NGC 619), the latter galaxy has an H I halo that is even more extended than that around NGC 612. In terms of star formation activity, the spectral synthesis modelling results of Holt et al. (2007) reveal young stellar populations of age <0.2 Gyr throughout the disc and bulge regions at NGC 612, and at MFIR wavelengths the source has a higher (LIRG-like) luminosity that other S0 galaxies of similar absolute brightness, suggesting a relatively high degree of ongoing star formation activity.

A0.3 3C 48

3C 48 was one of the first quasars to be optically identified and studied in detail. High-resolution radio maps show it to have complex radio structure that is relatively compact (Wilkinson et al. 1991, $D \sim 5$ kpc), while optical images reveal a large-scale tidal tail feature, evidence for a secondary nucleus, and amorphous, clumpy structures in the host galaxy envelope (Canalizo & Stockton 2000; Stockton et al. 2007). Long-slit spectra demonstrate that the latter are associated with young stellar populations with ages in the range

0.005–0.14 Gyr. 3C 48 has a higher MFIR luminosity than any other radio-loud AGN in our sample, qualifying it as a ULIRG; it also is significantly more luminous at 70 μm than other radio sources of similar [O III] luminosity (Dicken et al. 2009).

A0.4 Fornax A

The nearby FRI radio elliptical/S0 galaxy Fornax A shows a prominent, kpc-scale dust lane, as well as shells and other features on a larger scale. It is situated towards the edge of the Fornax cluster of galaxies, but it is not the dominant E/CD galaxy in the cluster. A line index analysis by Kuntschner (2000) gives a luminosity-weighted age of 2 Gyr for the stellar populations emitting the diffuse light of the galaxy. This is consistent with the 3 ± 0.5 Gyr obtained by Goudfrooij et al. (2001) using spectroscopic observations of three luminous clusters in the galaxy halo. Overall, the morphological and spectroscopic evidence supports the idea that this galaxy was involved in a major galaxy merger ~2–3 Gyr ago, associated with a period of enhanced star formation that formed the current intermediate-age stellar populations.

In order to attempt to learn more about the star formation history of Fornax A, we have carried out spectral synthesis modelling of our deep optical NTT spectrum of this source taken in 2003. Following the approach outlined in Holt et al. (2007) we have modelled the optical continuum SED using a combination of old (12.5 Gyr) and young (<5 Gyr) stellar populations, allowing for the possibility of reddening in the YSP. We find that, while YSPs are required to model the detailed shape of the continuum in the blue/near-UV, their flux contribution is relatively minor (<10 per cent at 4720 Å for a single burst YSP with age <1.0 Gyr). In consequence, the age and reddening of the YSP are not well constrained. For example, our fits to both the detailed absorption features and the overall SEDs are consistent with an old stellar population plus a minor (<5 per cent at 4720 Å) contribution from a YSP of age <0.1 Gyr, but they are also consistent with old stellar populations plus a more significant (>20 per cent at 4720 Å) contribution from an older YSP with age >1 Gyr (see Fig. A2); no range of ages for the YSP is ruled out. This illustrates the fact that it is difficult to accurately determine the age of a YSP that contributes relatively little to the overall optical light of a galaxy. Wider spectral coverage data, extending further into the UV, would be required to obtain more accurate results for Fornax A.

A0.5 PKS0409-75

PKS0409-75 is one of most luminous extragalactic radio sources in southern hemisphere (for $z < 1$), and also the most distant object in our sample. Despite its extreme radio luminosity, this source has only a moderate emission-line luminosity compared with other radio galaxies at similar redshifts. The deep i' image presented in Ramos Almeida et al. (2010a) shows a second galaxy of similar brightness 1.0 arcsec (9 kpc) to the east of the radio source host, and a number of galaxies of similar brightness within 150 kpc. Spectral synthesis modelling of a deep VLT optical spectrum of the integrated light of the host galaxy by Holt et al. (2007) demonstrates that a contribution from a YSP component of relatively young (<0.05 Gyr) age is required to model its SED accurately. Further evidence for recent star formation activity is provided by *Spitzer* observations which demonstrate that it has a high 70-μm luminosity for its (relatively modest) emission-line luminosity Dicken et al. (2009), as well as cool MFIR colours.
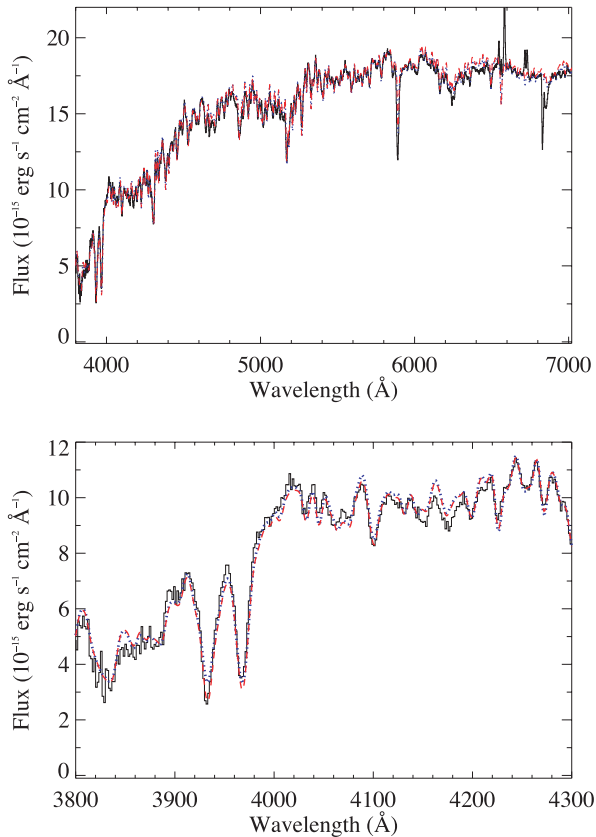
Figure A2. Spectral synthesis model fits to the nuclear spectrum of Fornax A. Top: Fits to the full spectral range. Bottom: Expanded plot showing the region around the 4000-Å break. The NTT spectroscopic data are shown in black, and two models are plotted: the red dotted line shows a model that comprises a 12.5-Gyr OSP a moderately reddened [$E(B - V) = 0.2$] YSP of age 2 Gyr that contribute 71.5 and 28.5 per cent of the light at 4770 Å, respectively; the blue dotted line shows a combination of an OSP (93.4 per cent) and a heavily reddened [$E(B - V) = 0.6$] YSP of age 0.05 Gyr (6.9 per cent). Note that both models provide an equally good fit to the data, despite the large difference in the YSP ages.

A0.6 B20648+27

This relatively low luminosity, compact radio source is surrounded by a spectacular ring structure of diameter ∼190 kpc, detected in both H I 21-cm and deep optical continuum observations (Emonts et al. 2006, 2008b). Spectral synthesis modelling of optical spectra of the disturbed elliptical host galaxy reveal a dominant flux contribution from an intermediate-age (0.3 ± 0.1 Gyr) YSP (Emonts et al. 2006).

A0.7 PKS0620-52

The deep r' image for PKS0620-52 presented in Ramos Almeida et al. (2010a) suggests that this FRI galaxy is the dominant cD galaxy in a rich cluster, a conclusion supported by the presence of a moderately luminous X-ray halo (Siebert et al. 1996; Trussoni et al. 1999). However, in this case there is no clear evidence for morphological disturbance, apart from the high incidence of nearby companion galaxies that is expected at the centre of a galaxy cluster. Spectral synthesis modelling by Wills et al. (2004) showed clear evidence for a YSP, although the relatively narrow spectral coverage and low S/N of their spectra precluded the determination of an

accurate age for the YSP. We have attempted to improve the determination of the properties of the YSP in this source by modelling a deeper, wider spectral coverage spectrum that was taken using the ESO 3.6-m telescope in 2007. Using the same modelling approach as described for Fornax A above, we find that we can obtain good fits to both the continuum SED and the detailed absorption line features for YSP ages <0.9 Gyr and reddening in the range $0 < E(B - V) < 1.5$ mag; older YSP ages are ruled out because they overpredict the strengths of the Ca II H+K absorption line features. It is not possible to determine the ages and reddening of the YSP more accurately for PKS0620-52 with the existing data, since the YSP make a relatively small contribution to the optical continuum (10–25 per cent at 4720 Å), although larger than in the case of Fornax A.

A0.8 3C 213.1

This intermediate redshift source shows a complex morphology at radio wavelengths, with a high surface brightness inner double structure (separation 17 kpc), along with a more diffuse and extended outer envelope of diameter ∼100 kpc. At optical wavelengths the source appears as a WLRG, and optical *HST* images reveal that the host galaxy has a distorted outer envelope (Wills et al. 2008). Spectral synthesis modelling demonstrates that a combination of a YSP of intermediate-age (0.4–0.8 Gyr) and low reddening and an OSP is required to model the spectrum of the nuclear regions of the host galaxy adequately.

A0.9 3C 218

This low-redshift radio source – also known as Hydra A – is situated in the Hydra cluster of galaxies. Despite its FRI radio morphology, with inner jets, edge-darkened structure on intermediate scales, and larger-scale diffuse structure that is only detected at low frequencies, Hydra A is one of the most powerful radio sources in the local Universe. Over recent years X-ray imaging observations of this source and its surrounding cluster, which show cavities in the hot ISM that coincide with the large-scale diffuse radio structure, have provided some of the best evidence that radio sources have a major impact on the thermal balance of the intracluster medium (Wise et al. 2007). At optical wavelengths the source has relatively weak emission lines considering its large radio power, and its optical continuum shows clear evidence for young stellar populations in the form of high-order Balmer lines and a Balmer break. Melnick, Gopal-Krishna & Terlevich (1997) have shown the latter to be associated with a rotating disc structure, also detected in emission lines. The deep r' image of this source presented in Ramos Almeida et al. (2010a) shows the extended diffuse halo expected of a central cluster galaxy, along with a kpc-scale dust lane in the central regions that is roughly co-aligned with the rotating disc structure detected by Melnick et al. (1997). The isophotes also show an elongation to the west of the nucleus in the direction of the dust lane. Modelling of the optical continuum by various authors yields a relatively young age for the YSP (∼0.05 Gyr: Aretxaga et al. 2001; Wills et al. 2004; Holt et al. 2007), which Holt et al. (2007) find to be moderately reddened.

A0.10 3C 236

A double–double radio source, with an inner compact structure of diameter 2 kpc along with a larger-scale radio source of diameter ∼4 Mpc, 3C 236 shows a disturbed optical morphology with twisted

isophotes and prominent dust lanes (Smith & Heckman 1989; de Koff et al. 2000). YSPs are detected in this source both photometrically (O'Dea et al. 2001) and spectroscopically (Holt et al. 2007). *HST* photometry of high surface brightness star formation regions in the galaxy provides evidence for two age ranges for the YSP ($\sim 10^7$ yr and 10^8–10^9 yr), perhaps associated with multiple outbursts of the radio source (O'Dea et al. 2001). However, spectral synthesis modelling of the spectrum of the integrated light of the central regions of the host galaxy by Holt et al. (2006) failed to provide a tight constraint on the age of the YSP ($t_{YSP} < 1$ Gyr), perhaps as a consequence of the relatively small flux contribution of YSP to the integrated light of the bulge of the galaxy, due to its relatively high reddening.

A0.11   3C 285

The host galaxy of this nearby FRII radio source shows a complex morphology at optical wavelengths, comprising a distorted S-shape envelope, tidal tails, fans and dust lanes (Heckman et al. 1986). Detailed observations of an irregular companion galaxy half-way between the nucleus and the eastern radio lobe of this source – Minkowski's object – provide some of the best evidence that star formation can be induced by interactions between radio jets and the ISM in radio source host galaxies (van Bruegel & Dey 1993; Croft et al. 2006). However, closer to the nucleus there are no signs that the YSP detected in optical spectroscopic observations by Aretxaga et al. (2001) and Holt et al. (2007) are associated with the radio structures. Modelling of optical spectra of the integrated light of the nuclear regions yields an intermediate age for the YSP (Holt et al. 2007).

A0.12   Centaurus A

The closest giant elliptical galaxy at a distance of only 3.5 Mpc, Centaurus A shows a complex radio morphology, comprising an inner high surface brightness edge-darkened structure with prominent radio jets, along with a more diffuse and highly extended outer double–double structure. At optical wavelengths the source has a prominent kpc-scale dust lane, as well as shells and discy isophotes on larger scales (Israel 1998); H I observations also reveal a ring of neutral gas of radius ~ 12 kpc (Schiminovich et al. 1994). Overall, the properties of the optical and H I features of Cen A are consistent with them originating in a galaxy merger. On the basis of dynamical studies, an age of between 0.2 and 0.75 Gyr is estimated for the central warped disc/dust lane structure (Quillen, Graham & Frogel 1993; Sparke 1996). In contrast, a comprehensive photometric and spectroscopic study of globular clusters in the halo of Cen A by Peng et al. (2004) reveals a population of metal-rich globular clusters with a significantly older mean age of 5^{+3}_{-2} Gyr. The latter are thought to have been formed in a merger between two disc galaxies that also produced the large-scale shells and discy isophotes. In addition, a blue tidal stream – probably a disrupted dwarf galaxy – has been discovered in NW halo of Cen A at a maximum radius of 8 kpc from the nucleus that has a spectroscopically confirmed age of ~ 0.35 Gyr (Peng et al. 2002). We discussed how these features may relate to the triggering of the radio jet activity in this complex system in Section 5.3 of the main paper.

A0.13   PKS1345+12

This radio morphology of this source shows a high surface brightness compact radio source of diameter ~ 0.2 kpc, along with a more diffuse radio source on larger scales (diameter: ~ 120 kpc:

Stanghellini et al. 2005). In optical images this object appears as a highly disturbed system, with a double nucleus of separation ~ 4.3 kpc, large-scale tidal tails and fans, and dust features; the AGN and radio jet activity are associated with the western nucleus of the system, which is driving powerful emission-line outflows (Holt, Tadhunter & Morganti 2003). Evidence for YSP in this system is provided both by the detection of young star clusters in the halo of the galaxy, and by spectral synthesis modelling of the diffuse light of the western nucleus and extended regions in the galaxy (Tadhunter et al. 2005; Rodríguez Zaurín et al. 2007, 2009). Photometric determination of the ages of the young star clusters using *HST* observations gives relatively young ages of 3–8 Myr, a result confirmed by the detection of stellar–photoionzed H II regions associated with the clusters. Remarkably, although the clusters are associated with dust lane features in the galaxy halo, they are moving large radial velocities relative to the ambient gas (Rodríguez Zaurín et al. 2007). The ages of the YSP detected in the diffuse light are less well determined because they contribute relatively little to the total flux; however, results for the nuclear aperture suggest relatively young ages (<0.1 Gyr). Further evidence for prodigious star formation activity in this source is provided by its MFIR luminosity, which qualify it as a ULIRG.

A0.14   3C 293

The radio morphology of 3C 293 is intermediate between FRI and FRII, with a high surface brightness inner structure of diameter 4 kpc that is offset by $42°$ relative to the lower surface brightness outer radio lobes; the total diameter of the extended radio source is 240 kpc. Displaying low-luminosity/ionization emission-line spectrum at optical wavelengths, its optical morphology is complex, with a series of dust lanes crossing the disc-like main body of the galaxy, and a large-scale tidal tail feature extending ~ 90 kpc from the nucleus that encompasses a companion galaxy ~ 32 kpc to the SE (Heckman et al. 1986; Smith & Heckman 1989). Despite the relatively low luminosity of its AGN as indicated by its optical emission lines, clear evidence for outflows is provided by the detection of broad, blueshifted H I 21-cm absorption and optical emission lines (Morganti et al. 2003; Emonts et al. 2005). The optical spectra presented in Tadhunter et al. (2005) show strong Balmer line absorption across the disc of the galaxy suggestive of intermediate-age young stellar populations, and spectral synthesis modelling gives YSP ages of ~ 0.1–2.5 Gyr (depending on aperture). Given the intermediate age and large mass of its YSP, 3C 293 would have appeared as a luminous- or ultraluminous infrared galaxy at the time of the starburst that formed the YSP, although its current far-IR luminosity is relatively modest.

A0.15   3C 305

The compact radio source 3C 305 has a distorted H-shaped radio morphology at radio wavelengths (Heckman et al. 1982) and, like 3C 293, shows evidence for outflows in the form of broad H I 21-cm absorption (Morganti et al. 2005). Other similarities with 3C 293 include: a discy optical morphology, dust lanes, large-scale tidal tails and a relatively massive, intermediate-age YSP (Heckman et al. 1986; Smith & Heckman 1989; Tadhunter et al. 2005).

A0.16   3C 321

Appearing as powerful FRII source on a large scale, 3C 321 has a relatively bright compact steep spectrum jet structure closer to the core. The jet structure passes close to the centre of a companion

galaxy situated only ∼3 arcsec to the NW of the nucleus of 3C 321 (Evans et al. 2008). Along with the double nucleus structure, other noteworthy features of 3C 321 at optical wavelengths include a dust lane in the main nucleus (de Koff et al. 2000) and large-scale tidal tail and fan structures (Heckman et al. 1986). Spectral synthesis modelling of the continuum spectra of both nuclei, the region in between, and the extended envelope of the galaxy to the SW (Holt et al. 2007), provide evidence for intermediate-age YSPs (see also Tadhunter, Dickson & Shaw 1996). This object also has a relatively large, LIRG-like luminosity at far-IR wavelengths.

A0.17 PKS1549-79

The radio source associated with the ULIRG PKS1549-79 has a compact, one-sided jet morphology, and a relatively flat radio spectrum. Optical observations demonstrate that the quasar nucleus in this object – detected at near-IR wavelengths – drives powerful outflows in the form of blueshifted high-ionization emission lines (Tadhunter et al. 2001; Holt et al. 2006). The optical morphology of the object is highly disturbed, with double tidal tails to the south of the nucleus, a jet-like feature of lower surface brightness to the north and evidence for dust lanes in the near-nuclear regions. (Holt et al. 2006; Batcheldor et al. 2007). Spectral synthesis modelling of the spectrum of the nuclear regions by (Holt et al. 2006) provided evidence for a YSP of relatively young age (0.04–0.1 Gyr). To refine the YSP age estimates, and look for possible spatial gradients, we have modelled the spectrum of an extended aperture of width 2 arcsec centred 2 arcsec (4.5 kpc) to the north of the nucleus along PA0. The latter was extracted from a VLT/FORS1 long-slit spectrum taken in excellent seeing conditions in 2003, and has the advantage that is much less affected by AGN-related continuum and emission line components than the nuclear aperture. We find that the age of the YSP in this extended region (0.06–0.08 Gyr: see Fig. A3) is entirely consistent with that determined in our earlier study of the nucleus.

A0.18 PKS1932-46

The BLRG PKS1932-46 shows an FRII morphology at radio wavelengths Villar-Martín et al. (1998), and is situated ∼100 kpc from a prodigiously star-forming companion galaxy of similar redshift to the NE (Inskip et al. 2007). The deep r' image for this source
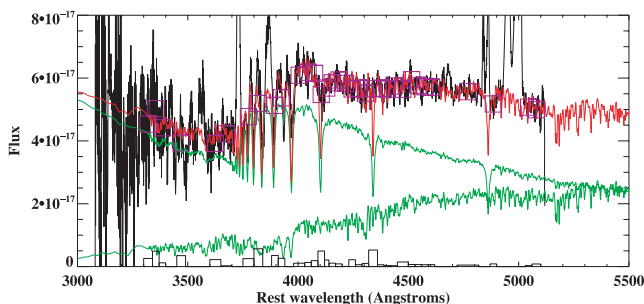
Figure A3. Spectral synthesis modelling results for the extended aperture in PKS1549-79 (see text for details). The black solid line represents the data, while the red line shows the model, which comprises a combination of an unreddened 0.06-Gyr YSP (upper green curve) and an unreddened 12.5-Gyr OSP (lower green curve). The YSP and the OSP contribute 60 and 40 per cent of the total flux at 4720 Å, respectively. The boxes show the continuum bins used for the fit, while the histogram at the bottom shows the magnitudes of the residuals from the fit in each bin.

presented in Ramos Almeida et al. (2010a) shows an amorphous structure in the envelope of the elliptical host galaxy, as a well as an extraordinary series of interlinked arc structures to the N of the galaxy, that point to, but do not quite connect with, a tail/arm feature emanating from the NE companion galaxy. Spectral synthesis modelling of the nuclear spectrum of the host galaxy does not provide unambiguous evidence for a YSP, in part because of the contamination by strong AGN continuum emission associated with the BLRG nucleus (Holt et al. 2007). However, deep VLT spectra reveal a highly extended emission line nebula extended in an N–S direction with line ratios consistent with photoionization by hot stars, rather than by the AGN. This provides direct evidence for an extended population of very young (<10 Myr) stars in the halo of the galaxy (Villar-Martín et al. 2005).

A0.19 PKS2135-209

This compact steep spectrum radio source ($D \sim 3$ kpc) shows clear evidence for both a quasar nucleus and young stellar populations in its optical spectrum (Tadhunter et al. 2002; Holt et al. 2007). Therefore, it can be classified as a post-starburst quasar (see Brotherton et al. 1999). The deep i' image presented in Ramos Almeida et al. (2010a) shows that it lies in a relatively isolated environment, and its host galaxy has a distorted outer envelope. Due to the presence of the strong quasar emission in the optical spectrum of this object, it is not possible to determine the age of its YSP accurately: both young (<0.1 Gyr) and intermediate (0.1–0.6 Gyr) ages are consistent with detailed fits to the continuum SED and detailed absorption features. Further evidence for prodigious recent star formation in this source is provided by its ULIRG-like far-IR luminosity and relatively cool far-IR colours (Dicken et al. 2009).

A0.20 3C 433

The radio structure of 3C 433 is highly distorted (van Breugel et al. 1983), with steep spectrum jets close to, and on either side of, the nucleus on an N–S axis, along with extended radio lobes to the N and S that show highly asymmetric, low-surface-brightness tail features to the east (N lobe) and west (S lobe); the south lobe is also much brighter than the north lobe. Optical images and spectra show another early-type galaxy of similar brightness and redshift 14 kpc to the NE of the nucleus of 3C 433, and an amorphous envelope that is crossed with patchy dust absorption features (de Koff et al. 1996, 2000). Detailed modelling of long-slit optical continuum spectra reveals evidence for YSP in the host galaxy of 3C 433, the companion galaxy to the NE, and the region in between (Wills et al. 2002; Holt et al. 2007). However, the age of the YSP is only well constrained in the nuclear spectrum of the host galaxy, for which relatively young YSP ages ($0.03 < t_{YSP} < 0.1$ Gyr) and moderate reddening [$0.4 < E(B - V) < 0.7$] are deduced (Holt et al. 2007).

A0.21 3C 459

In terms of its radio morphology, 3C 459 appears as an asymmetric, relatively compact ($D \sim 27$ kpc) FRII source on large scales, but also shows evidence for a relatively bright compact steep spectrum core (Thomasson, Saikia & Muxlow 2003). The deep r' image for this source presented in Ramos Almeida et al. (2010a) reveals fan-like protrusions to the south of the nucleus of the galaxy, while

high-resolution *HST* images show a series of compact knots extending to a radius of 4 kpc from he nucleus (Wills et al. 2008). Of all the sources considered in this paper, 3C 459 is the object in which YSPs make the largest proportional contribution to the optical spectrum, with strong Balmer absorption lines, Balmer break and He I absorption lines detected in its nuclear spectrum. This has allowed its YSP to be modelled in unprecedented detail. The results shown in Table 2 are for a model comprising a reddened YSP and an OSP (consistent with the modelling approach used for most of the other objects shown in Table 2). They reveal a dominant contribution from a relatively young YSP of age 0.04–0.07 Gyr (Wills et al. 2008) and modest reddening. However, although the simple YSP+OSP model provides a useful indication of the luminosity-weighted age of the YSP component, we find that we can obtain better fits for a combination of reddened young and intermediate-age YSPs with ages 0.004–0.005 Gyr (40 per cent), 0.04 Gyr (35 per cent) and 0.5–0.9 Gyr (25 per cent). The extended apertures in this source give similar results. This is one of the five sources in our sample with a ULIRG-like far-IR luminosity. Note that, in common with most ULIRGs (see Rodríguez Zaurín et al. 2009), we can model the spectra of this source adequately without any contribution from an OSP.

This paper has been typeset from a TEX/LATEX file prepared by the author.